Given the previous clinical and experimental evidence, we hypothesized that the cardiac sympathetic nerve density dramatically changes with the acceleration of circulating NE concentration and subsequently affects the cardiac performance. To test this hypothesis in vivo, we carried out the present study to examine the temporal association of NGF expression in the heart and cardiac sympathetic nerve density during the development of CHF in the continuous NE-infused rats.

2. Materials and Methods

2.1. Animal experiments

Seven-week old male Wistar rats weighting 240 to 260 g (CLEA Japan,Inc.) were divided into two experimental groups; (1) vehicle-infusion as control groups and (2) NE-infused rats. 0.9% saline with ascorbate (1 mmol/L) vehicle or (-)norepinephrine bitartrate (Sigma Chemical Co.) dissolved in 0.9% saline with ascorbate (1 mmol/L) was administered continuously by subcutaneously implanted osmotic mini pumps (ALZET Osmotic Pumps, model 2004) into the interscapular region. Rats were sedated with ketamine (60 mg/kg) and xylasine (15 mg/kg) given intraperitoneally. NE was infused at a rate of 0.05 mg/kg/hr for maximum 28 days. The animals were killed at 0-, 1-, 3-, 7-, 14-, and 28-day after implantation of osmotic pumps. On the day of the experiment, rats were artificially ventilated under anesthesia with ketamine (60 mg/kg) and xylasine (60 mg/kg) given intraperitoneally. A catheter (HAKKO disposable ELASTER TYPE2, 25G × 38 mm) filled with heparin-saline solution, connected to a pressure transducer, was inserted into the thoracic aorta and left ventricle (LV) through the right carotid artery to measure aortic pressure and LV pressure. Mean arterial pressure, LV pressure, LV dp/dt, LV –dp/dt, and heart rate were recorded using a polygraph system (Nihon Kohden). A blood sample (1.5 ml) was then collected from the carotid arterial catheter for measuring plasma NE. The rats were then killed and their hearts, lungs, livers, and left stellate ganglia were removed. Each heart (LV + septum), lung, and liver was weighted. To establish mice that selectively expressed enhanced green fluorescent protein (EGFP) in sympathetic nerves, mice carrying a reporter gene construct chicken β-actin promoter (CAG)-chloramphenicol acetyl transferase (CAT)-EGFP (Kawamoto et al., 2000) were crossed with a mouse line expressing Cre recombinase under the control of the dopamine β-hydroxylase (DBH) promoter (Matsushita et al., 2004). The CAG-CAT EGFP transgenic mouse was a gift from J. Miyazaki (Osaka University, Osaka, Japan). The DBH-Cre recombinase transgenic mouse was provided by K. Kobayashi (Fukushima Medical University, Fukushima, Japan). Five-week-old DBH-Cre/Floxed-EGFP mice were implanted osmotic mini pumps (ALZET Osmotic Pumps, model 2004) into the interscapular region under above-mentioned anesthesia. NE was infused at a rate of 0.05 mg/kg/hr for maximum 28 days. Vehicle-infusion mice were used as controls. The animals were killed at 28-day after implantation of osmotic pumps. All animal experiments approved by the Animal Care and Use Committee of the Keio University.

2.2. Plasma NE measurement

Blood samples were collected in iced heparin-treated tubes containing EDTA-2Na (1 mg/ml) and centrifuged (500 × g) at 4 °C for 10 min. Plasma was aliquoted and stored at -20 °C until subsequent assay. NE was assayed by high-performance liquid chromatography (HPLC) with electrochemical detection as described previously (Hjemdahl, 1984).

2.3. Tissue NE measurement

Tissue samples were homogenized within 30 sec in 0.1 N HCl containing 0.1% sodium pyrosulfite (Na2S2O5). After centrifugation (10000 g, 30 min), NE was extracted with alumina and determined by HPLC.

2.4. RNA extraction and poly(A)$^+$RNA Northern Blot Analysis

Total RNA from frozen rat tissue samples (LV + septum) was extracted using TRIzol Reagent (GIBCO BRL), and poly(A)$^+$RNA was isolated. Rat NGF, BNP, and glyceraldehyde-3-phosphate dehydrogenase (GAPDH) cDNA were obtained by RT-PCR from the heart and cloned into the pCRα plasmid. GAPDH cDNA was used as an internal control. Inserts were labeled with [α-^{32}P]dCTP by the random priming technique. A 2.5 μg sample of poly(A)$^+$RNA was run on a 1% MOPS/formaldehyde-agarose gel, and Northern blots were performed as described previously (Sano et al., 2000).

2.5. Immunohistochemical procedures

Sample fixation, embedding, sectioning, and blocking were as described previously (Mabe et al., 2006). To detect nerve fibers in the heart, frozen sections were incubated with double antibodies against protein gene product 9.5 (PGP9.5) (Ultraclone UK, RA95101; 1:2000), growth-associated protein (GAP43) (CHEMICON, AB5220; 1:4000), tyrosine hydroxylase (TH) (CHEMICON, AB152; 1:200), or GFP (Medical&Biological Laboratories, 598; 1:500) and α-Actinin (Sigma, A7811; 1:800). The following secondary antibodies were used: Alexa Fluor 488-conjugated donkky anti-rabbit IgG (Molecular Probes; 1:200), polyclonal swine anti-rabbit TRITC (DAKO; 1:200), Alexa Fluor

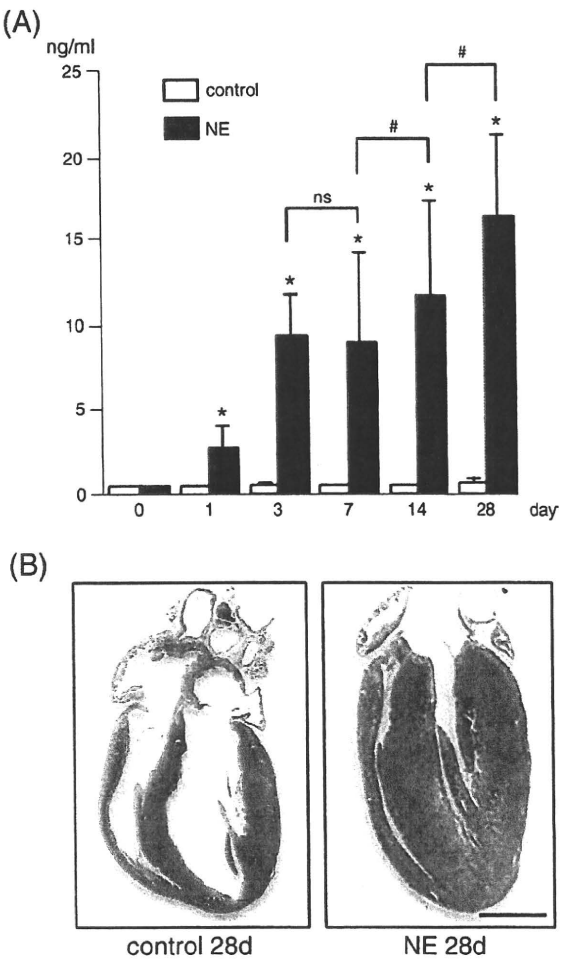

Fig. 1. (A) Plasma concentrations of NE in control and NE-exposed rat. *p<0.01 compared to control at same day, #p<0.01, ns: not significant. (B) Representative section along the long-axis of heart from control and NE-exposed rats at 28-day stained by HE. Note that the LV is markedly thickened and the LV cavity is narrowed. Scale bar indicates 4 mm.

Table 1
Mean wet weight of the tissues in control and NE-treated rats.

	BW (g)	LV+S(mg)	LV+S /body weight (10^{-3})	Lung(mg)	Lung /body weight (10^{-3})	Liver(mg)	Liver /body weight (10^{-3})
Day 0							
Control (n=7)	248±9	565±49	2.3±0.3	1178±226	4.8±0.4	8320±149	33.5±0.8
NE (n=8)	259±11	549±25	2.1±0.1	1184±88	4.6±0.7	8470±135	32.7±0.8
Day 1							
Control (n=8)	245±9	569±17	2.4±0.1	1154±154	4.7±0.7	8286±136	33.8±0.8
NE (n=14)	254±13	571±38	2.3±0.1	1163±115	4.6±0.9	8433±457	33.2±1.6
Day 3							
Control (n=8)	267±8	622±41	2.3±0.1	1195±125	4.5±0.5	8619±195	32.3±1.1
NE (n=15)	258±12	647±64	2.6±0.3	1173±271	4.5±0.5	8590±223	33.3±1.7
Day 7							
Control (n=8)	273±11	635±17	2.3±0.1	1243±221	4.5±0.6	8872±123	32.5±0.9
NE (n=12)	267±12	782±72*	2.9±0.3*	1287±169	4.8±0.6	8663±198	32.4±2.2
Day 14							
Control (n=8)	289±10	638±41	2.2±0.1	1397±153	4.8±0.7	8940±114	30.9±0.4
NE (n=13)	270±18	862±97*	3.1±0.3*	1375±224	5.1±0.4	8897±251	33.0±1.7
Day 28							
Control (n=8)	306±13	710±16	2.3±0.1	1473±246	4.8±0.8	9117±108	29.8±0.4
NE (n=20)	317±21	983±88*	3.2±0.2*	1538±184	4.8±0.9	9430±322	28.8±2.5

*:p 0.01 vs. control.

488-conjugated goat anti-mouse IgG (Molecular Probes; 1:200), and Alexa Fluor 546-conjugated goat anti-mouse IgG (Molecular Probes; 1:200). Apoptosis was measured by using a TUNEL assay kit (Promega). The samples were observed under a Zeiss LSM 510 META confocal microcopy (Germany). Immunostained areas were quantified using NIH image, as described previously (Cao et al., 2000).

2.6. Statistics

Values are presented as means±SD. The significance of differences among mean values was determined by ANOVA. Statistical comparison of the control group with treated group was carried out using the non-parametric Fisher's multiple comparison tests. The level accepted for significance was $p<0.05$.

3. Results

3.1. Plasma NE concentration

To begin with, to address the characterization of continuous NE infusion model, we measured the plasma NE concentration in the control and NE infusion rats. Plasma NE concentration in NE-treated rats was significantly increased from 1-day after administration compared with control rats. Although the plasma NE level once reached a plateau at around 9 ng/ml between 3-and 7-day, it started to increase after that and finally reached to 16.1±5.6 ng/ml at 28-day (control level was 0.39±0.1 ng/ml, $p<0.01$) (Fig. 1A).

Table 2
Hemodynamic measurements.

	Mean BP (mmHg)	LVEDP (mmHg)	dP/dt (mmHg / sec)	-dP/dt (mmHg / sec)	HR (bpm)
Day 0					
Control (n=7)	112±4	2.5±0.6	9410±529	6133±643	316±16
NE (n=8)	103±6	2.9±0.5	9267±416	6318±306	306±24
Day 1					
Control (n=8)	114±15	3.0±0.6	9333±503	6267±416	316±17
NE (n=14)	123±9	3.0±0.6	9250±632	6105±469	332±25
Day 3					
Control (n=8)	118±6	3.1±0.5	9366±423	5917±402	324±30
NE (n=15)	125±21	5.5±1.4	9467±372	6334±501	339±31
Day 7					
Control (n=8)	108±16	2.9±0.4	9067±306	5967±153	311±9
NE (n=12)	127±10	6.7±1.2*	8120±415	5114±458	343±32
Day 14					
Control (n=8)	103±3	2.9±0.5	9305±436	5907±265	311±9
NE (n=13)	131±23*	7.9±1.5*	6114±460*	4771±594	349±25
Day 28					
Control (n=8)	110±4	3.4±0.6	9467±416	6008±296	316±17
NE (n=20)	143±19*	15±1.9*	5843±476*	3729±419*	360±20*

*:p 0.01 vs. control.

3.2. Appearance and weights

The representative photograph of the longitudinal section of the whole heart in the control and NE-treated rats at 28-day were shown in Fig. 1B. Left ventricular (LV) wall was markedly thickened, and LV cavity was narrowed. Right ventricular free wall was also thickened compared with the control, but less conspicuous than LV. Then, the whole body, LV free wall with septum (S) (LV+S), lung, and liver were separately weighed, and were shown in Table 1. The ratio of LV+S/body weight

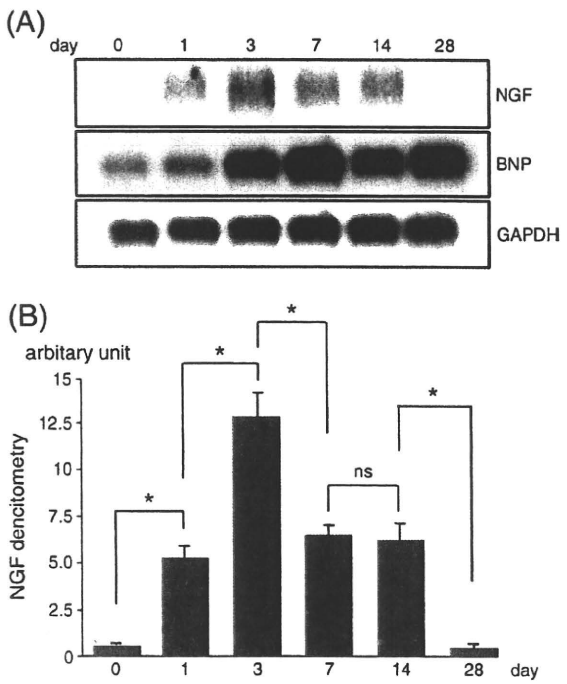

Fig. 2. (A) Northern blot analysis of NGF, BNP, and GAPDH in the left ventricle of NE-exposed rats. (B) Dencitometry analysis of NGF mRNA expression. Northern blot analysis was repeated three times. Expression of NGF mRNA was upregulated at 3-day, subsequently downregulated, and finally almost disappeared at 28-day. *p<0.01, ns: not significant.

(BW) increased from 7-day, and reached by 1.39-fold of the control rats at 28-day. NE-treated rats at-28 day had pleural effusion and ascites. This was the reason why the BW of NE-treated rats at 28- day turned to increase, although those at 14-day decreased compared with control. That was also the cause of unchanged ratio of lung/BW and liver/BW between two groups at 28-day, whereas both lung and liver weight themselves in NE-treated rats were increased. Similarly, the ratio of LV + S/BW in NE-treated rats at 28-day should be much greater than that of controls. These findings indicated that NE treatment for 28 days induced decompensated LV hypertrophy (LVH).

3.3. Hemodynamic measurements

Mean blood pressure of NE-treated rats began to increase at 1-day after NE exposure, significantly increased at 14-day, and reached at 143 ± 19 mmHg (control; 110 ± 4 mmHg) at 28-day (Table 2). LV end-diastolic

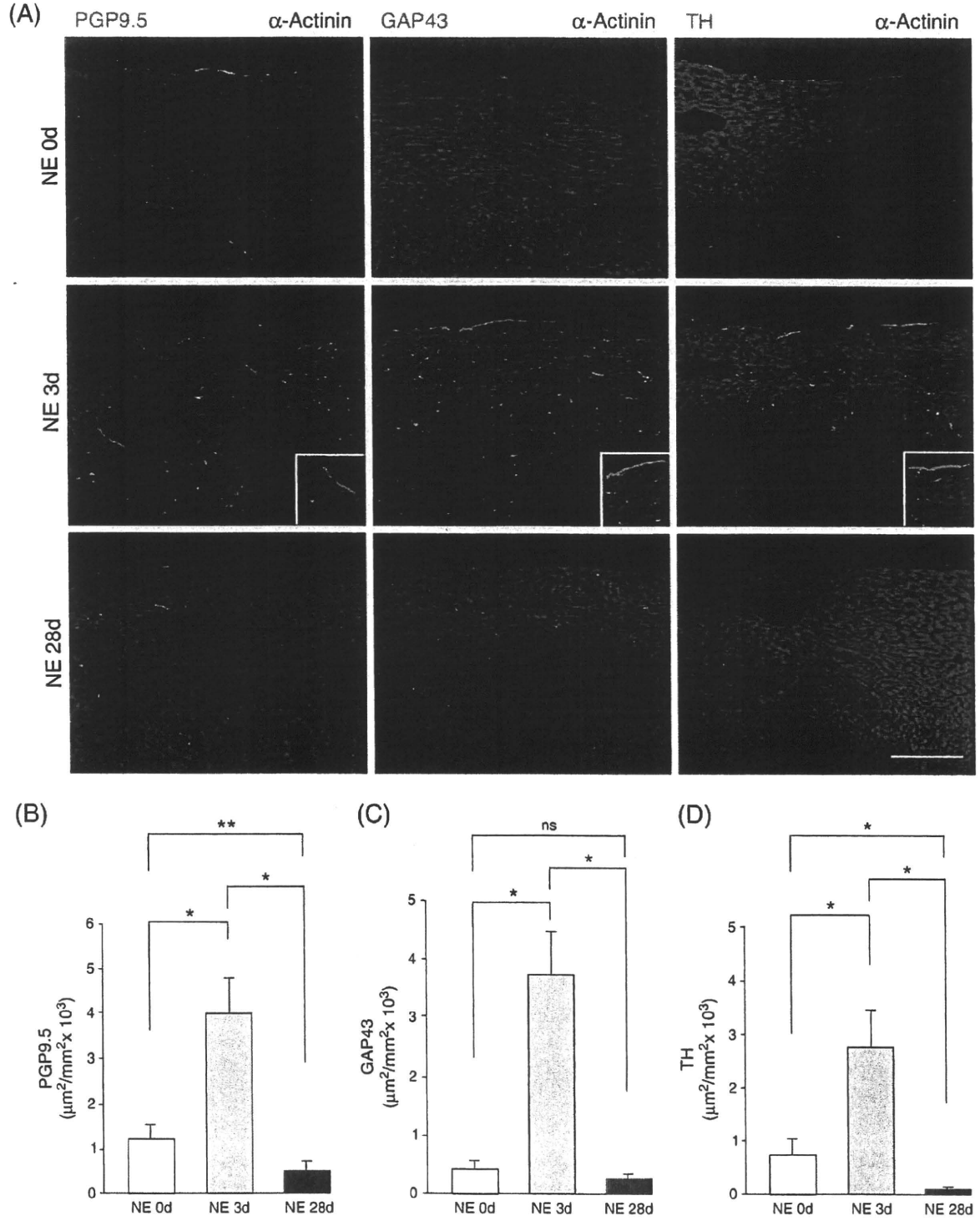

Fig. 3. (A) Double-immunofluorescent staining for PGP9.5, GAP43, and TH with α-Actinin in the LV of 0-, 3-, and 28-day after NE infusion. Insets show high magnification of each sample. (B, C, D) Quantitative analysis of the immunostained area for PGP9.5 (B), GAP43 (C), and TH (D). Scale bar indicates 200 μm. *$p<0.01$, **$p<0.05$, ns: not significant.

pressure (LVEDP) of NE-treated rats started to be raised at 3-day and markedly increased up to 15 ± 1.9 mmHg (control; 3.4 ± 0.6 mmHg) at 28-day. Although it was not significant, it was noteworthy that both dP/dt and |−dP/dt| were temporally elevated in NE-exposed rats at 3-day, whereas these were significantly attenuated at 14-day. Heart rates in NE-infused rats were significantly higher than control at 28-day. These data indicated that NE treatment for 28 days induced heart failure model caused by pressure-overload and/or catecholamine injury.

3.4. NGF and BNP mRNA expression in LV

The performance of NGF mRNA expression in LV of NE-infused rats was immensely unique. In briefly, NGF mRNA was prominently augmented at 3-day after exposure of NE, and after that, it was down-regulated and almost completely disappeared at 28-day. It showed biphasic change through the 28 days. On the other hand, BNP mRNA expression was predictably increased proportionally with the augmentation of LVEDP (Fig. 2 and Table 2).

3.5. Immunohistochemistory for nerve density in heart section

Levels of NGF expression within innervated tissue roughly correspond to innervation density. Thus, we performed an immunohistochemical staining of protein gene product 9.5 (PGP9.5), growth associated protein 43 (GAP43) and tyrosine hydroxylase (TH) to evaluate the nerve density. The PGP9 5 is specifically expressed in nerve fiber axon. GAP43 is a protein that was expressed when the nerve terminal develops. TH is an enzyme that catalyzes the conversion of L-tyrosine to L-DOPA and is a rate-determining enzyme for catecholamine synthesis. For this reason, it is used as a marker of sympathetic nerves. Interestingly, there was a remarkable increase in the expression of PGP9.5, GAP43, and TH in the LV at 3-day after administration of NE. Newly developed nerves were prominent at the

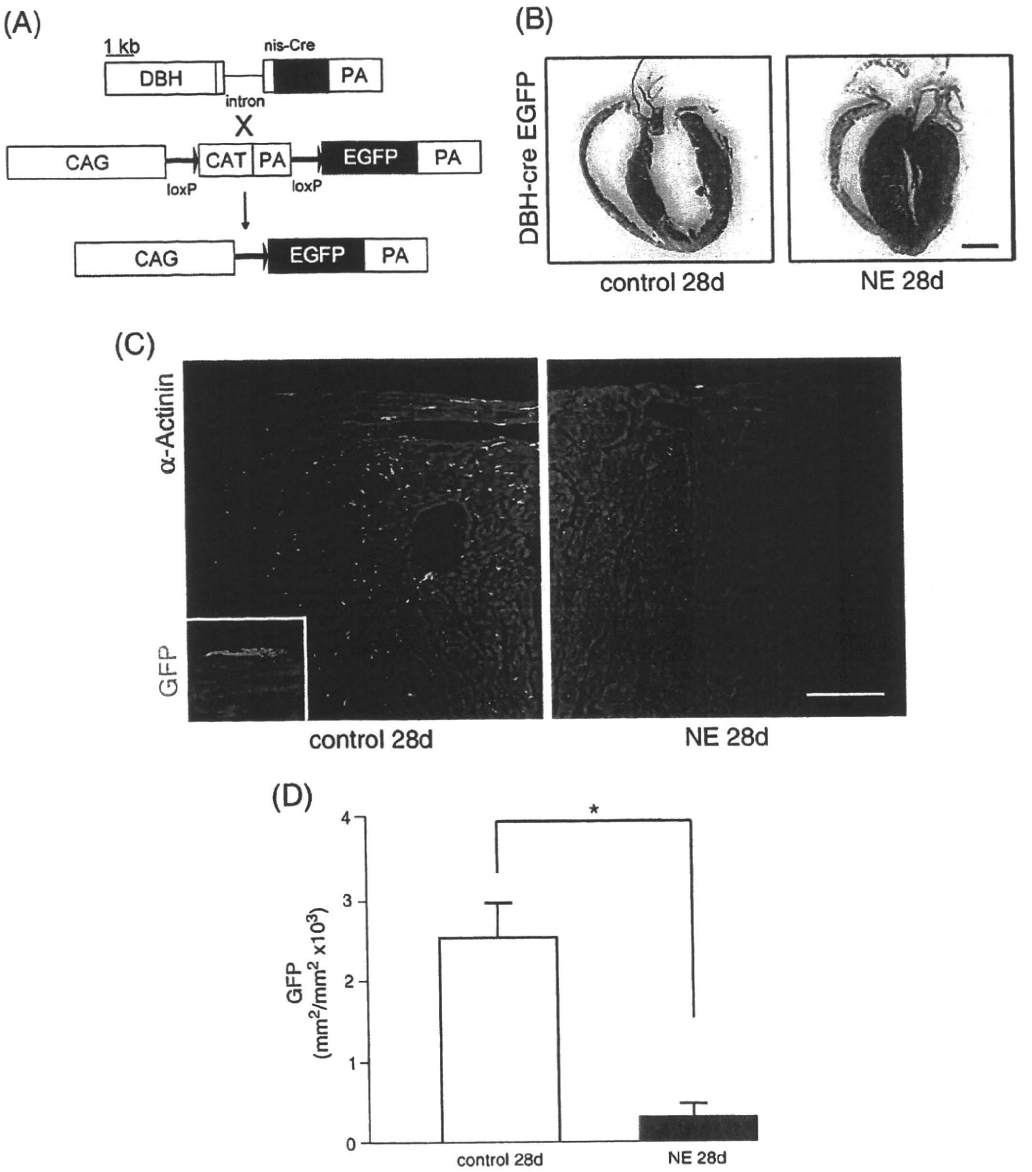

Fig. 4. (A) Dopamine β-hydroxylase (DBH)-Cre transgenic mice were crossed with CAG-CAT-EGFP mice. In the double-transgenic mice ($Cre^+/EGFP^+$), Cre-loxP recombination deletes the CAT gene cassette, leading to the expression of EGFP in sympathetic neurons. (B) Representative section of heart along the long axis from control and NE-infused mice (28-day) stained by HE. Scale bar indicates 2 mm. (C) Double- immunofluorescent staining for GFP and α-Actinin in the LV of control and NE-infused mice at 28-day. Inset shows high magnification. Scale bar indicates 200 μm. (D) Quantitative analysis of the immunostained area for GFP in the LV of control and NE-infused mice. *$p<0.01$.

epicardial layer or the perivascular area, indicated sympathetic neurons (Fig. 3A). The quantitative analysis revealed that PGP9.5, GAP43, and TH increased 3.2-fold, 9.1-fold, and 3.8-fold respectively, in LV at 3-day after NE administration compared with 0-day. (Fig. 3B, C, D). In contrast, not only growth cone marker GAP43 -immunostained neurons, but also nerve fiber marker PGP9.5-immunostained neurons were conspicuously down-regulated in decompensated hypertrophic LV at 28-day (Fig. 3A). The quantitative analysis revealed that the immunostained area of PGP9.5 and TH at 28-day decreased by 88% and 95%, respectively of that at 3-day and also decreased by 58% and 88%, respectively of that at 0 day. The immunostained area of GAP43 at 28-day down-regulated by 92% of that at 3- day, but there was no significant difference between 0-day and 28-day (Fig. 3B, C). These data indicated that sympathetic nerve density in LV was directly correlated with the NGF expression.

3.6. Cardiac sympathetic nerve density in NE-infused mice using the Cre-LoxP system

To confirm whether cardiac sympathetic nerve density is truly attenuated by long-time exposure of NE, we next prepared double-transgenic conditional knockouts by crossing mice carrying a floxed CAT- CAG- EGFP allele with mice that expressed Cre recombinase under the control of the DBH promoter (Fig. 4A), and subjected them to continuous NE infusion to induce heart failure. The adrenergic cells of brain, adrenal, and stellate ganglia in these mice showed a strong GFP signal (data not shown). Longitudinal sections of the whole heart in NE-infused mice at 28-day showed a marked LVH (Fig. 4B). NE-treated mice at 28-day had systemic effusion, indicating that they were in the decompensated stage of heart failure. Immunostaining revealed that GFP signal were markedly decreased in the LV in NE-injected mice at 28-day (Fig. 4C), with the positively stained areas for GFP in the LV following NE-infusion decreased by 87% compared to controls (Fig. 4D). These data confirmed that long-term NE administration causes the anatomical cardiac sympathetic denervation concomitant with severe heart failure.

3.7. Tissue NE content in LV

The NE that is present in the heart is located in the sympathetic nerve fibers rather than in the myocardium per se. To investigate the alteration of sympathetic nerve density could correspond to the sympathetic terminal NE stores, we measured the NE content of the LV tissue in the control and NE-exposed rats. The NE content at 3-day in the LV of the NE-exposed rats tremendously increased 2.1-fold compared with the control at 3- day, sequentially down-regulated, and markedly decreased at 28-day (Fig. 5). These data indicated that the NGF-dependent sympathetic innervation greatly influenced the patterning of the tissue NE content in the LV and LV performance estimated by dP/dt and -dP/dt (Fig. 5 and Table 2).

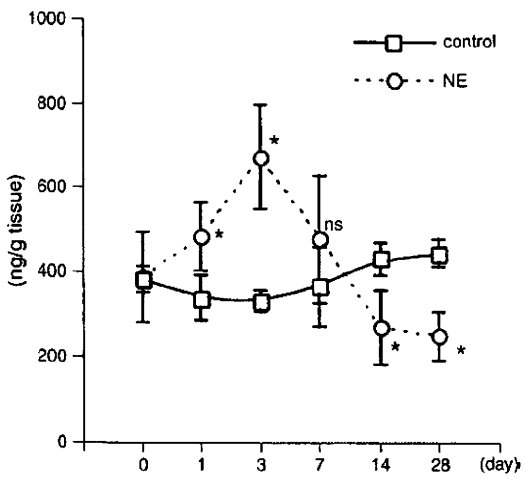

Fig. 5. Tissue NE concentrations in the LV of control and NE-infused rats. *$p<0.01$ compared to control at same day. ns: not significant between control and NE-infused at 7-day.

3.8. Analysis of neuronal cell bodies in stellate ganglion

To investigate whether NE-toxicity directly affects the apoptosis of sympathetic nerve cell body in stellate ganglion, we examine TUNEL assay and count the number of neuronal cell bodies at 0-, 3-, and 28-day in NE-infused rats. The small number of TUNEL positive cells was only observed in the interstitial cells, but not in the neuronal cell bodies at either 0-, 3-, or 28-day (Fig. 6A). Moreover, the number of neuronal cell bodies in stellate ganglion was not significantly different among 0-, 3-, and 28-day (Fig. 6B).

4. Discussion

4.1. Character of NE-infusion model

Continuous NE administration by osmotic pump effectively maintained the high plasma NE concentration throughout 28 days in rats. The level of the concentration reached to a plateau at 3-day after exposure, maintaining the level until 7-day, however it seemed to exceed the estimated value at 28-day. It is generally known that in patients with advanced heart failure, the circulating NE concentration is higher than the level found in normal subjects (Meredith et al., 1993). In our model at 28-day, the higher plasma NE level was presumably modified by heart failure, that is to say, NE induced NE release. As evidenced by the retention of pleural effusion and ascites accompanied with weight gain and the prominent increase of LVEDP, the NE- infused rats at 28-day presented decompensated phase of heart failure. The mean blood pressure of NE-infused rats at 28 day was significantly increased, however compared with the other high blood pressure model, e.g. transaortic constriction mouse or Dahl salt sensitive rat, the level was not enough to produce pressure overload induced heart failure (Sheikh et al., 2008; Miyachi et al., 2009). For the reason of these, we estimated the main etiology of cardiomyopathy in this model as a result of NE induced cardiac injury with hypertrophy directly derived from NE.

4.2. Sympathetic hyper-innervation phase towards hypertrophy

The cardiac performance of NE-exposed rats temporally accelerated at 3 day. Around this phase, cardiac muscles were started to be driven by the increasing circulatory NE via β1 adrenergic receptors. Moreover, at that time, we confirmed that NE content in the sympathetic nerve terminal was also upregulated, reasonably accompanied by sympathetic hyperinnervation. Locally released NE from hyperinervated nerve terminals was presumably more effective in controlling cardiac performance than circulatory NE (Chang et al., 1991). Needless to say, NE itself is a strong cardiac hypertrophic factor and it also derives other hypertorphic factors, e.g. endothelin-1(ET-1), angiotensin II, leukemia inhibitory factor (LIF), from cardiomyocytes (Okada et al., 1995; Baker et al., 1990; Wang et al., 2001). Among these factors, ET-1 has been proven as a factor which can induce NGF expression in cardiomyocytes via ET-A receptor/Giβγ pathway (Ieda et al., 2004). In this study, we observed the augmented NGF expression in the LV of NE-infused rat at 3-day. Although we did not examine the expression of ET-1 in this study, we speculated that the augmented expression of NGF was presumably elicited by ET-1. This speculation is strongly supported by the study of Kaddoura et al. They reported that ventricular expression of ET-1 mRNA is elevated in the first 3 days and falls after that in NE-infused rat (Kaddoura et al., 1996). Moreover, we recently reported that the augmented NGF mRNA expression concomitant with upregulated ET-1 mRNA causes cardiac sympathetic hyperinnervation in pressure-

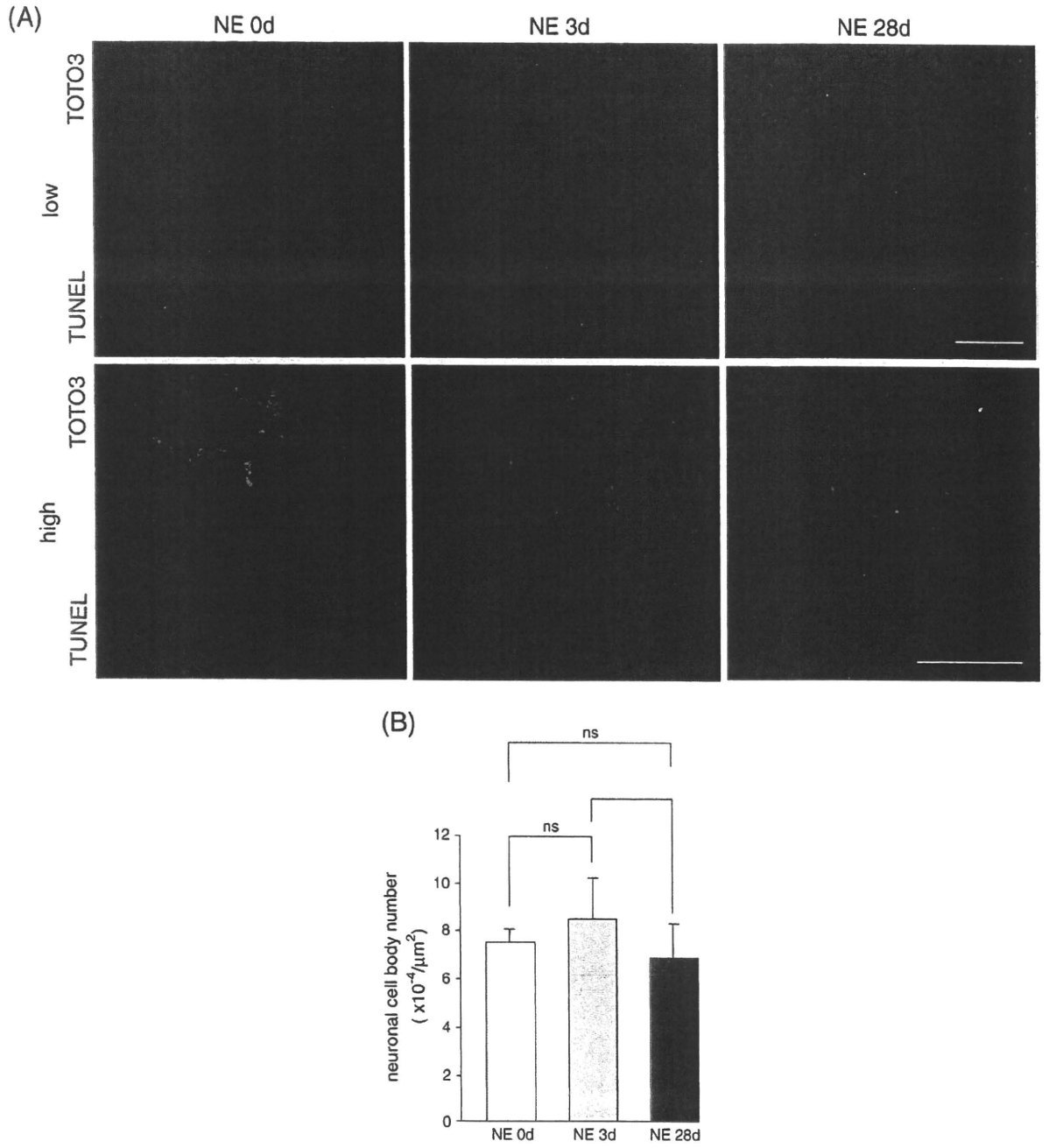

Fig. 6. (A) TUNEL staining in left stellate ganglion of 0-, 3-, and 28-day after NE infusion. Upper panels show low magnification (scale bar indicates 50 μm) and lower panels show high magnification (scale bar indicates 100 μm). (B) Quantitative analysis of the neuronal cell body number in the stellate ganglion in 0-, 3-, and 28-day (n = 5, respectively) of NE-infused mice. ns: not significant.

overload induced cardiac hypertrophy (Kimura et al., 2007). It is noteworthy that the number of neuronal cell bodies in stellate ganglion was not significantly increased at 3-day after NE infusion, indicating the sympathetic fibers were sprouted from the peripheral knots by the augmented NGF expression.

Taken together, our data indicated that the cardiac hyperinnervation induced by the enhanced NGF expression influenced the facilitation of cardiac performance in the early period of NE-infused animals.

4.3. Sympathetic denervation phase during heart failure

In our study, the NGF mRNA expression was enormously down-regulated concomitant with the high plasma concentration in NE-infused rats at 28-day. This resulted in the cardiac sympathetic denervation and attenuated tissue NE contents. We also clearly showed that cardiac sympathetic fibers were markedly reduced in NE-induced heart failure mice, in which sympathetic nerves could be traced by EGFP. Furthermore, we showed no clear evidence of that NE-toxicity directly affects apoptosis of sympathetic neurons in stellate ganglion. These results suggest that long- exposure of NE causes the NGF depletion in the heart, which secondary affects the retreating of peripheral sympathetic fibers from the heart. Our results are strongly supported by the following two studies. Qin et al. reported that NE-mediated reduction of NGF and its neurotrophic receptor tyrosine kinase A (TrkA) involve in the decrease of sympathetic neurotransmitter in heart failure in vivo (Qin et al., 2002). Kaye et al. reported NE

exposure reduced NGF expression in isolated cardiomyocytes (Kaye et al., 2000). Although direct correlation between NGF level and sympathetic nerve density has not been examined in these papers, they showed that TrkA expression and tyrosine hydroxylase profile were decreased in CHF and NE-infused animals, indicating sympathetic denervation. The mechanism of NE induced NGF downregulation in vivo still remains unexplained. In vitro study, Kaye showed the reduced NGF expression is achieved by 10 μmol NE via α-adrenergic receptor-coupled protein kinase C signal pathway (Kaye et al., 2000). This NE concentration in the medium is almost 100 times higher than the plasma concentration of our NE-infusion model at 28-day, whereas we presume that the myocardial injury dependent on NE-exposed time and dose might affect the several gene expressions which regulate NGF production from cardiomyocytes in vivo. Recently, Rana et al showed that mechanical stretch and α-1-adrenergic stimulation attenuate the NGF expression via the calcineurin-NFAT signaling pathway in cultured neonatal cardiomyocyte (Rana et al., 2009). The renin-angiotensin-aldosterone system is also activated in heart failure, however, little is known as to how it affects the NGF reduction in severe heart failure. Additional studies are needed to investigate the precise mechanism in vivo.

4.4. Significance from clinical viewpoint

Many studies demonstrated a high plasma NE concentration concomitant with a depressed MIBG reuptake in CHF, and this phenomenon has been explained as sympathetic denervation (Henderson et al., 1988). A general definition of denervation seems to include two meanings. One is functional denervation. As we know, NE uptake activity in sympathetic nerve ends is reduced in CHF, and this is considered as a general mechanism in attenuated MIBG reuptake. Elevated NE level is attributed in the development of cardiac sympathetic nerve terminal abnormalities in CHF (Bohm et al., 1995). And we have recently reported that pressure overload induces the rejuvenation of cardiac sympathetic nerve and LIF and cardiotrophin-1, derived from failing heart, give rise to the cholinergic transdifferentiation in cardiac sympathetic nerve via gp130 signaling pathway, causing the functional sympathetic denervation in CHF (Kimura et al., 2007, Kanazawa et al., 2010).

Second is anatomical denervation, which is more rigorous definition of the word. In this study, we demonstrated that long-exposure of high plasma concentration of NE caused myocardial NGF reduction, following peripheral sympathetic fiber loss in severe CHF animals. Moreover, nerve loss and reduced NE content in cardiac tissue obviously indicated that plasma NE elevation in severe CHF is derived from peripheral organs, but not a spillover from the cardiac sympathetic nerve ends.

We speculated that functional sympathetic denervation precedes anatomical denervation and the latter could be observed in the advanced stage of heart failure accompanied with long-exposure of high plasma NE. Because our previous study showed that the augmentation of LIF and cardiotrophin-1 in failing heart rather than NGF reduction affects the cardiac sympathetic function via cholinergic transdifferentiation in heart failure models, such as transaortic constriction mice and Dahl salt sensitive rats (Kanazawa et al., 2010). In these conventional models, duration and level of the high plasma NE concentration might be insufficient to affect the NGF reduction.

In human severe CHF, there are huge evidence that protective therapy against catecholamine-toxicity improve cardiac function and prognosis. We are interested in how β-blocker therapy may affect these processes in sympathetic nerve loss.

Furthermore, as we showed, the cardiac NGF depletion did not result in the neuronal cell death, which occurred to us that NGF supplement therapy might be effective for the improvement in cardiac function in severe CHF (Kreusser et al., 2006). We are also interested in the influence of high plasma NE concentration on parasympathetic neurons. Further, it has been known that sympathetic denervation is also observed in diabetic heart. Although it could be explained by depletion of the neurotrophic factors, little is known about the precise mechanism in diabetic neuropathy. Thus, further studies will be required to investigate the peculiar mechanism of cardiac denervation in each disease.

Acknowledgements

This study was supported in part by the research grants (10B-1) of "Nervous and Mental Disorders from the Ministry of Health and Welfare" and research grants from the Ministry of Education, Science and Culture, Japan, and Health Science Research Grants for Advanced Medical Technology from the Ministry of Welfare, Japan.

References

Baker, K.M., Chernin, M.I., Wixson, S.K., Aceto, J.F., 1990. Renin-angiotensin system involvement in pressure-overload cardiac hypertrophy in rats. Am. J. Physiol. 259, H324–H332.

Bohm, M., La Rosee, K., Schwinger, R.H., Erdmann, E., 1995. Evidence for reduction of norepinephrine uptake sites in the failing human heart. J. Am. Coll. Cardiol. 25, 146–153.

Cao, J.M., Fishbein, M.C., Han, J.B., Lai, W.W., Lai, A.C., Wu, T.J., Czer, L., Wolf, P.L., Denton, T.A., Shintaku, I.P., Chen, P.S., Chen, L.S., 2000. Relationship between regional cardiac hyperinnervation and ventricular arrhythmia. Circ. 101, 1960–1969.

Chang, P.C., Kriek, E., van der Krogt, J.A., van Brummelen, P., 1991. Does regional norepinephrine spillover represent local sympathetic activity? Hypertens. 18, 56–66.

Cohn, J.N., Levine, T.B., Olivari, M.T., Garberg, V., Lura, D., Francis, G.S., Simon, A.B., Rector, T., 1984. Plasma norepinephrine as a guide to prognosis in patients with chronic congestive heart failure. N Engl J. Med. 311, 819–823.

Eisenhofer, G., Friberg, P., Rundqvist, B., Quyyumi, A., Lambert, G., Kaye, D., Kopin, I., Goldstein, D., Esler, M., 1996. Cardiac sympathetic nerve function in congestive heart failure. Circ. 93, 1667–1676.

Hasking, G.J., Esler, M.D., Jennings, G.L., Burton, D., Korner, P.I., 1986. Norepinephrine spillover to plasma in patients with congestive heart failure: evidence of increased overall and cardiorenal sympathetic nervous activity. Circ. 73, 615–621.

Henderson, E.B., Kahn, J.K., Corbett, J.R., Jansen, D.E., Pippin, J.J., Kulkarni, P., Ugolini, V., Akers, M.S., Hansen, C., Buja, L.M., 1988. Abnormal I-123 metaiodo-benzylguanidine myocardial washout and distribution may reflect myocardial adrenergic derangement in patients with congestive cardiomyopathy. Circ. 78, 1192–1199.

Heumann, R., Korsching, S., Scott, J., Thoenen, H., 1984. Relationship between levels of nerve growth factor (NGF) and its messenger RNA in sympathetic ganglia and peripheral target tissues. EMBO J. 3, 3183–3189.

Himura, Y., Felten, S.Y., Kashiki, M., Lewandowski, T.J., Delehanty, J.M., Liang, C.S., 1993. Cardiac noradrenergic nerve terminal abnormalities in dogs with experimental congestive heart failure. Circ. 88, 1299–1309.

Hjemdahl, P., 1984. Catecholamine measurements by highperformance liquid chromatography. Am. J. Physisl. 247, E13–E20.

Ieda, M., Fukuda, K., Hisaka, Y., Kimura, K., Kawaguchi, H., Fujita, J., Shimoda, K., Takeshita, E., Okano, H., Kurihara, Y., Kurihara, H., Ishida, J., Fukamizu, A., Federoff, H.J., Ogawa, S., 2004. Endothelin-1 regulates cardiac sympathetic innervations in the rodent heart by controlling nerve growth factor expression. J. Clin. Investig. 113, 876–884.

Kaddoura, S., Firth, J.D., Boheler, K.R., Sugden, P.H., Poole-Wilson, P.A., 1996. Endothelin-1 is involved in norepinephrine-induced ventricular hypertrophy in vivo. Circ. 93, 2068–2079.

Kanazawa, H., Ieda, M., Kimura, K., Arai, T., Kawaguchi-Manabe, H., Endo, J., Kawakami, T., Kimura, T., Monkawa, T., Hayashi, M., Iwanami, A., Shimoda, K., Okano, H., Okada, Y., Ishibashi-Ueda, H., Ogawa, S., Fukuda, K., 2010. Heart failure causes cholinergic transdifferentiation of cardiac sympathetic nerves via gp130-mediated cytokines. J. Clin. Investig. 120, 408–421.

Kawamoto, S., Niwa, H., Tashiro, F., Sano, S., Kondoh, G., Takeda, J., Tabayashi, K., Miyazaki, J., 2000. A novel reporter mouse strain that expresses enhanced green fluorescent protein upon Cre-mediated recombination. FEBS Lett. 470, 263–268.

Kaye, D.M., Vaddadi, G., Gruskin, S.L., Du, X.J., Esler, M.D., 2000. Reduced myocardial nerve growth factor expression in human and experimental heart failure. Circ. Res. 86, 80–84.

Kimura, K., Ieda, M., Kanazawa, H., Yagi, T.K.T., Tsunoda, M.N.S., Kurosawa, H., Yoshimi, K., Mochizuki, H., Yamazaki, K., Okada, Y., Ogawa, S., Fukuda, K., 2007. Cardiac sympathetic rejuvenation: a link between nerve function and cardiac hypertrophy. Circ. Res. 100, 1755–1764.

Kreusser, M.M., Haass, M., Buss, S.J., Hardt, S.E., Gerber, S.H., Kinscherf, R.K., Katus, H.A., Backs, J., 2006. Injection of nerve growth factor into stellate ganglia improves norepinephrine reuptake into failing hearts. Hypertens. 47, 209–215.

Mabe, A.M., Hoard, J.L., Duffourc, M.M., Hoover, D.B., 2006. Localization of cholinergic innervation and neurturin receptors in adult mouse heart and expression of the neurturin gene. Cell Tissue Res. 326, 57–67.

Matsushita, N., Kobayashi, K., Miyazaki, J., Kobayashi, K., 2004. Fate of transient catecholaminergic cell types revealed by site-specific recombination in transgenic mice. J. Neurosci. Res. 78, 7–15.

Meredith, I., Eisenhofer, G., Lambert, G., Dewar, E., Jennings, G., Esler, M., 1993. Cardiac sympathetic nervous activity in congestive heart failure: evidence for increased neuronal norepinephrine release and preserved neuronal uptake. Circ. 88, 136–145.

Miyachi, M., Yazawa, H., Furukawa, M., Tsuboi, K., Ohtake, M., Nishizawa, T., Hashimoto, K., Yokoi, T., Kojima, T., Murate, T., Yokota, M., Murohara, T., Koike, Y., Nagata, K., 2009. Exercise training alters left ventricular geometry and attenuates heart failure in dahl salt-sensitive hypertensive rats. Hypertens. 53, 701–707.

Okada, M., Yamashita, C., Okada, M., Okada, K., 1995. Role of endothelin-1 in beagles with dehydromonocrotaline-induced pulmonary hypertension. Circ. 92, 114–119.

Packer, M., Bristow, M.R., Cohn, J.N., Colucci, W.S., Fowler, M.B., Gilbert, E.M., Shusterman, N.H., 1996. The effect of carvedilol on morbidity and mortality in patients with chronic heart failure. N Engl J. Med. 334, 1349–1355.

Pool, P.E., Covell, J.W., Levitt, M., Gigg, J., Braunwald, E., 1967. Reduction of cardiac tyrosine hydroxylase activity in experimental congestive heart failure: its role in the depletion of cardiac norepinephrine stores. Circ. Res. 20, 349–353.

Qin, F., Vulapalli, R.S., Stevens, S.Y., Liang, C.S., 2002. Loss of cardiac sympathetic neurotransmitters in heart failure and NE infusion is associated with reduced NGF. Am. J. Physiol. 282, H363–H371.

Rana, O.R., Saygili, E., Meyer, C., Gemein, C., Krüttgen, A., Andrzejewski, M.G., Ludwig, A., Schotten, U., Schwinger, R.H.G., Weber, C., Weis, J., Mischke, K., Rassaf, T., Kelm, M., Schauerte, P., 2009. Regulation of nerve growth factor in the heart: The role of the calcineurin-NFAT pathway. J. Mol. Cell. Cardiol. 46, 568–578.

Sano, M., Fukuda, K., Kodama, H., Pan, J., Saito, M., Matsuzaki, J., Takahashi, T., Makino, S., Kato, T., Ogawa, S., 2000. Interleukin-6 family of cytokines mediate angiotensin II-induced cardiac hypertrophy in rodent cardiomyocytes. J. Biol. Chem. 275, 29717–29723.

Sheikh, F., Raskin, A., Chu, P.H., Lange, S., Domenighetti, A.A., Zheng, M., Liang, X., Zhang, T., Yajima, T., Gu, Y., Dalton, N.D., Mahata, S.K., Dorn II, G.W., Heller-Brown, J., Peterson, K.L., Omens, J.H., McCulloch, A.D., Chen, J., 2008. An FHL1-containing complex within the cardiomyocyte sarcomere mediates hypertrophic biomechanical stress responses in mice. J. Clin. Investig. 118, 3870–3880.

Snider, W.D., 1994. Functions of the neurotrophins during nervous system development: what the knockouts are teaching us. Cell 77, 627–638.

Thomas, J.A., Marks, B.H., 1978. Plasma norepinephrine in congestive heart failure. Am. J. Cardiol. 41, 233–243.

Wang, F., Seta, Y., Baumgarten, G., Engel, D.J., Sivasubramanian, N., Mann, D.L., 2001. Functional significance of hemodynamic overload-induced expression of leukemia-inhibitory factor in the adult mammalian heart. Circ. 103, 1296–1302.

Am J Physiol Renal Physiol 299: F648–F655, 2010.
First published April 14, 2010; doi:10.1152/ajprenal.00402.2009.

Cyclic stretch induces proliferation and TGF-β1-mediated apoptosis via p38 and ERK in ureteric bud cells

Hisayo Fujita,[1] Mariko Hida,[1] Katsuyoshi Kanemoto,[3] Keiichi Fukuda,[2] Michio Nagata,[3] and Midori Awazu[1]

Departments of [1]Pediatrics and [2]Regenerative Medicine and Advanced Cardiac Therapeutics, Keio University School of Medicine, Tokyo; and [3]Department of Molecular Pathology, Institute of Basic Medical Sciences, Graduate School of Comprehensive Human Sciences, University of Tsukuba, Ibaraki, Japan

Submitted 16 July 2009; accepted in final form 8 April 2010

Fujita H, Hida M, Kanemoto K, Fukuda K, Nagata M, Awazu M. Cyclic stretch induces proliferation and TGF-β1-mediated apoptosis via p38 and ERK in ureteric bud cells. *Am J Physiol Renal Physiol* 299: F648–F655, 2010. First published April 14, 2010; doi:10.1152/ajprenal.00402.2009.—We previously reported that p38 mitogen-activated protein kinase (p38) and phosphorylated ERK are upregulated in cyst epithelium of human renal dysplasia and obstructive uropathy in fetal lambs (Omori S, Fukuzawa R, Hida M, Awazu M. *Kidney Int* 61: 899–906, 2002; Omori S, Kitagawa H, Koike J, Fujita H, Hida M, Pringle KC, Awazu M. *Kidney Int* 73: 1031–1037, 2008). Dysplastic epithelium is characterized by proliferation, apoptosis, and upregulation of Pax2 and transforming growth factor (TGF)-β1. In the present study, we investigated whether cyclic mechanical stretching of ureteric bud cells, a mimic of the hydrodynamic derangement after fetal urinary tract obstruction, reproduces events seen in vivo. Cyclic stretch activated p38 and ERK and upregulated Pax2 expression in a time-dependent manner in ureteric bud cells. Stretch-stimulated Pax2 expression was suppressed by a p38 inhibitor, SB203580, or a MEK inhibitor, PD98059. 5-Deoxyuridine incorporation was increased by stretch at 24 h, which was also abolished by SB203580 or PD98059. On the other hand, apoptosis was not induced at 24 h by stretch but was significantly increased at 48 h. TGF-β1 secretion was increased by stretch at 24 h, which was inhibited by SB203580 or PD98059. Inhibition of p38 or ERK as well as anti-TGF-β antibody abolished the stretch-induced apoptosis. Finally, exogenous TGF-β1 induced apoptosis of ureteric bud cells, which was inhibited by SB203580 and PD98059. In conclusion, cyclic stretch induces Pax2 upregulation, proliferation, and TGF-β1-mediated apoptosis, features characteristic of dysplastic epithelium, via p38 and ERK in ureteric bud cells.

dysplastic kidney; obstructive uropathy; kidney development; cell signaling

MITOGEN-ACTIVATED PROTEIN kinases (MAPKs) are enzymes that play important roles in various cellular functions including proliferation, differentiation, and apoptosis. MAPKs are developmentally regulated in the rat kidney (22). Thus p38 MAPK (p38) and ERK are strongly expressed in the fetal kidney, whereas JNK is detected predominantly in the adult kidney. MAPKs play an important role in the development of both normal and abnormal kidneys. The inhibition of p38 or ERK by specific inhibitors in organ-cultured kidneys results in disturbed nephron formation, indicating their importance in the early stages of kidney development (11). On the other hand, the persistent fetal expression pattern of MAPKs, i.e., upregulation of p38 and ERK and downregulation of JNK, is observed in cyst epithelium of human renal dysplasia and an ovine model of fetal obstructive uropathy, suggesting that dysregulated MAPKs may lead to kidney malformation (20, 23).

Renal dysplasia is the major cause of chronic renal failure in children (37). It is characterized by primitive-appearing dysplastic tubules connected to cysts and surrounding peritubular and pericystic fibromuscular collars (31). Urinary tract obstruction often accompanies dysplastic kidneys and is suggested to contribute to the pathogenesis. In animals, prenatal obstruction of the urinary tract reproduces dysplastic changes, and in utero relief of obstruction prevents abnormal renal differentiation (7, 25). Upregulation of a transcription factor, Pax2, and proapoptotic and profibrotic cytokine, transforming growth factor (TGF)-β1, as well as proliferation and apoptosis are characteristic features of dysplastic epithelium (2, 38–41).

In urinary tract obstruction, tubules are mechanically stretched (27). Renal tubular epithelium senses and responds to mechanical stretch via the activation of ion channels and subsequent increases in intracellular calcium levels. Calcium influxes activate a number of signaling molecules, including MAPKs (1, 27). Mechanical stretch also leads to the activation of downstream effectors of renal injury such as TGF-β1 and apoptotic responses (17–19). Although it is not known whether mechanical stretch stimulates proliferation of renal tubule cells, it does stimulate proliferation in a variety of cells via MAPKs in some cases (29). The mechanisms of Pax2 upregulation and the coexistence of increased proliferation and apoptosis, characteristics of dysplastic epithelium, remain to be elucidated. In the present study, therefore, we investigated whether cyclic stretch recapitulates features seen in in utero urinary tract obstruction using ureteric bud (UB) cells in an attempt to clarify the sequence of events leading to the generation of dysplasia. Using UB cells is highly relevant for examining the role of cell stretch in fetal urinary tract obstruction, since renal dysplasia is hypothesized to be caused by malformed development of UBs (26). Also, we used UB cells as a representative of immature tubule cells seen during kidney development. Although UB cells eventually differentiate into collecting ducts, they possess characteristics common to immature tubules such as increased proliferation, expression of Pax2, and activation of p38 and ERK (2, 21, 23).

MATERIALS AND METHODS

Reagents. Antibodies against phosphorylated p38 (P-p38) and P-ERK were from Cell Signaling Technology (Beverly, MA). Anti-p38 (C-20) was from Santa Cruz Biotechnology (Santa Cruz, CA). Anti-ERK (Erk1/2-CT, rabbit polyclonal IgG) was from Upstate

Address for reprint requests and other correspondence: M. Awazu, Dept. of Pediatrics, Keio Univ. School of Medicine, 35 Shinanomachi, Shinjuku-ku, Tokyo 160-8582, Japan (e-mail: awazu@sc.itc.keio.ac.jp).

Biotechnology (Lake Placid, NY). Rabbit anti-Pax2 was from Zymed Laboratories (South San Francisco, CA). Monoclonal mouse anti-TGF-β1, -β2, -β3 antibody and human TGF-β1 were from Genzyme (Cambridge, MA). Horseradish peroxidase-conjugated anti-mouse IgG and anti-rabbit IgG were from Amersham (Buckinghamshire, UK). Normal mouse IgG and collagen type I, rat tail was from Upstate Biotechnology. A p38 inhibitor, SB203580, and a MEK inhibitor, PD98059, were from Carbiochem-Novabiochem (La Jolla, CA). DMEM, FBS, penicillin, streptomycin, Hanks' balanced salt solution, and trypsin-EDTA were from GIBCO Laboratories (Grand Island, NY). Hoechst 33258 was from Polyscience (Warrington, PA).

Cell culture and mechanical stretch. The UB cell line generated from mice transgenic for SV40 T-antigen was a generous gift of Dr. J. Barasch. Cells were grown in DMEM containing 10% FBS, and were plated at a density of 1×10^5 cells/cm^2 on silicone rubber dishes precoated with collagen (10 μg/cm^2). Cells were serum deprived for 24 h and then stretched (20% elongation, 20 cycles/min unless otherwise indicated) for 10 min-48 h using a computer-driven cell-stretching device (Research Instruments Development Division, Keio University School of Medicine). In the experiments to inhibit p38, ERK, or TGF-β1, cells were incubated with 5 μM SB203580, 5 μM PD98059, or 30 μg/ml anti-TGF-β antibody. The cultures were maintained at 37°C in a humidified atmosphere of 95% O_2-5% CO_2.

Immunoblot analysis. After 0–48 h of stretching, cells were washed with cold PBS and lysed in solubilization buffer containing 20 mM HEPES (pH 7.2), 1% Triton X-100, 10% glycerol, 20 mM sodium fluoride, 1 mM sodium orthovanadate, 1 mM PMSF, 10 μg/ml aprotinin, and 10 μg/ml leupeptin. Insoluble material was removed by centrifugation (10,500 *g*, 10 min). The protein content in cell lysates was measured with a DC protein assay (Bio-Rad Laboratories, Tokyo, Japan). Lysates were resolved by SDS-PAGE and transferred to polyvinylidene difluoride membranes (Immobilon, Millipore, Bedford, MA). Nonspecific binding sites were blocked in TBS buffer (10 mM Tris·HCl, pH 7.4, 0.15 M NaCl) containing 0.1% Tween 20 and 5% skim milk overnight at 4°C or for 1 h at 25°C. Antibodies were added to TBS containing 0.1% Tween 20 in saturating titers and incubated with mixing for 2 h at 25°C. Bound antibodies were detected using the ECL Western blotting system (Amersham, Arlington Heights, IL). Blots were scanned and quantitatively analyzed by ImageJ software.

Cell proliferation. 5-Deoxyuridine (BrdU) incorporation was measured by a cell proliferation ELISA system (Amersham). BrdU was added to the incubation media, and then cells were stretched in the presence or absence of 5 μM SB203580 or 5 μM PD98059 for 24 h. After fixation and blocking, cells were incubated with peroxidase-labeled anti-BrdU antibody for 90 min. After washes, tetramethyl benzidine was added. The absorbance of samples was measured at 450 nm.

TGF-β1 assay. Cells were stretched in the presence or absence of SB203580 or PD98059 for 24 h. TGF-β1 in the media was measured using ELISA kits (Quantikine; R&D Systems). To activate TGF-β1, samples were acidified with 1 N HCl, incubated at room temperature for 10 min, and neutralized with 1.2 N NaOH. Samples were measured according to the manufacturer's instructions.

Cell apoptosis. Cells were stretched in the presence or absence of SB203580, PD98059, or anti-TGF-β antibody for 24 or 48 h or incubated with 5 ng/ml TGF-β1 for 24 h. Apoptosis was assessed by morphology using Hoechst 33258.

RT-PCR analysis. Total RNA was collected from cells using TRIzol reagent (Invitrogen, Carlsbad, CA): Reverse transcription was performed with 2 μg of the total RNA using Oligo dT primer and Moloney murine leukemia virus reverse transcriptase (Invitrogen). The primers are forward 5′-CCG AAT ACA AGC GAC AGA ACC-3′ and reverse 5′-TCA CCG TTG GAG CGA GGA ATC-3′ for Pax2, and forward 5′-CCT GCA AGA CCA TCG ACA TG-3′ and reverse 5′-ACT CAG GCG TAT CAG TGG GG for TGF-β1. Conditions for amplifications are as follows: following a 5-min denaturation at 95°C, 30 cycles consisting of 95°C for 1 min, 55°C (Pax2), or 58°C (TGF- β1) for 1 min, and 72°C for 1 min, with a final extension of at 72°C for 7 min. GAPDH was used as an internal standard. PCR products were resolved by agarose gel electrophoresis and visualized with ethidium bromide.

Statistical analysis. The results are expressed as means ± SE. Statistical analysis was performed with ANOVA followed by multiple comparisons as appropriate. Statistical significance was determined as $P < 0.05$.

RESULTS

Cyclic stretch activates p38 and ERK in a cycle- and time-dependent manner in UB cells. Cyclic stretching of UB cells with 20% elongation at 10 cycles/min for 24 h significantly increased P-p38 and P-ERK compared with unstretched cells (Fig. 1). The phosphorylation of p38 and ERK was further increased by stretching cells at 20 cycles/min. For subsequent experiments, therefore, cells were stretched at 20 cycles/min unless otherwise indicated. We next examined the time course of stretch-dependent activation of p38 and ERK. Cyclic stretch induced a biphasic elevation of P-p38 with a rapid early peak at 10 min, although not statistically significant, followed by a second time-dependent increase (Fig. 2*A*). The increase was significant at 24 and 48 h (Fig. 2, *A* and *B*). In a similar manner to p38, ERK1 and ERK2 phosphorylation tended to increase at 10 min and again at 2 h, with increasing levels toward 24 h. The phosphorylation was significantly increased 6–24 h after the initiation of stretch, and was sustained at least up to 48 h (Fig. 2, *C* and *D*). The initial transient increase in P-p38 and P-ERK may be a stress response. Total p38 and ERK protein levels were unaltered by stretch throughout the course.

Cyclic stretch increases Pax2 expression via p38 and ERK in UB cells. Two isoforms of Pax2 were detected by immunoblot analysis in UB cells. Cyclic stretch increased Pax2 expression in a time-dependent manner, with a significant 1.7-fold increase at 24 h (Fig. 3*A*). Pax2 was also increased at the mRNA level by stretch (Fig. 3*B*). Coincubation with p38 inhibitor SB203580 or MEK inhibitor PD98059 abolished both the baseline and cyclic stretch-induced in Pax2 expression (Fig. 3, *C* and *D*). Since levels of P-p38 or P-ERK in

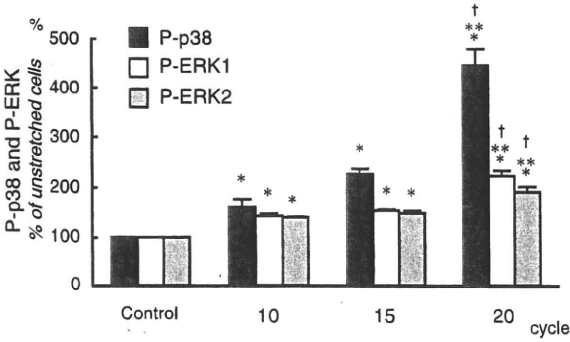

Fig. 1. p38 and ERK are activated by cyclic stretch in a cycle-dependent manner in ureteric bud cells. Ureteric bud cells were stretched 10–20 cycles/min for 24 h. Equal amounts of lysates (60 μg) were loaded and immunoblotted with anti-phospho-p38 (P-p38) or anti-phospho-ERK (P-ERK) antibody. Values are means ± SE; $n = 5$. *$P < 0.05$ vs. control. **$P < 0.05$ vs. 10 cycles/min. †$P < 0.05$ vs. 15 cycles/min.

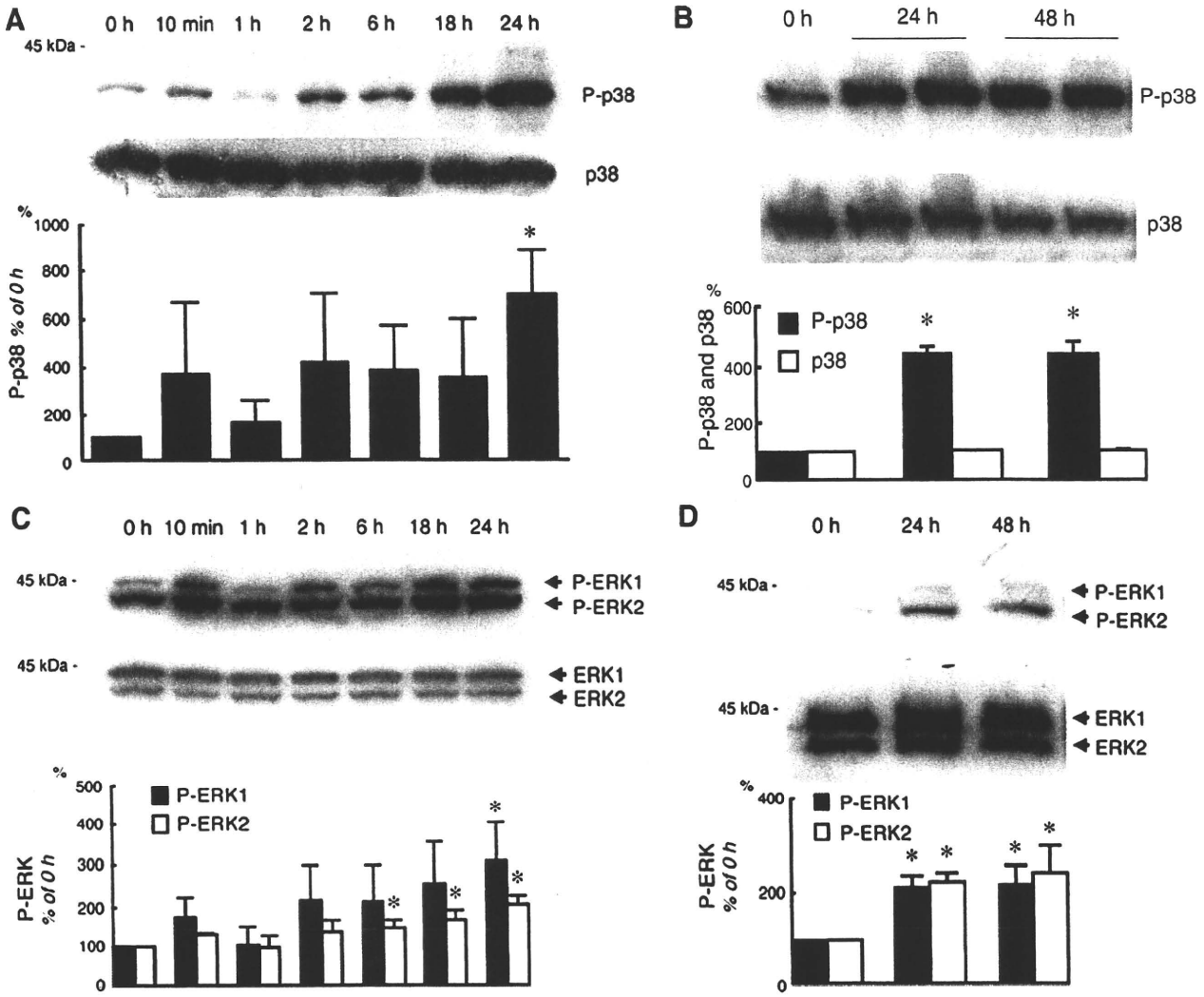

Fig. 2. p38 and ERK are activated by cyclic stretch in a time-dependent manner in ureteric bud cells. Ureteric bud cells were stretched 20 cycles/min for 0–48 h. Equal amounts of lysates (60 μg) were loaded and immunoblotted with anti-P-p38, anti-p38 (*A* and *B*), anti-P-ERK, or anti-ERK antibody (*C* and *D*). Representative immunoblots and quantitative analyses are shown. Values are means ± SE; $n = 3$. *$P < 0.05$ vs. 0 h.

SB203580- or PD98059-treated unstretched cells, respectively, were less than those in unstretched control cells, and since those in SB203580- or PD98059-treated stretched cells were equal to those in unstretched control cells, Pax2 expression is thought to be regulated by p38 and ERK.

Cyclic stretch increases BrdU incorporation via p38 and ERK in UB cells. We next examined whether cyclic stretch stimulates proliferation of UB cells. BrdU incorporation was increased 1.9-fold in cells stretched for 24 h compared with unstretched cells ($P < 0.05$, Fig. 4). Stretch-induced BrdU incorporation was completely inhibited by coincubation with SB203580 or PD98059, demonstrating that the proliferation was mediated by p38 and ERK.

Cyclic stretch induces TGF-β1 secretion via p38 and ERK in UB cells. We then examined whether cyclic stretch stimulates secretion of TGF-β1, a mediator of fibrosis in urinary tract obstruction. The amount of total (latent and active) TGF-β1 in the medium of cells stretched for 24 h was significantly increased compared with that of unstretched cells (Fig. 5*A*). TGF-β1 mRNA was also increased by stretch (Fig. 5*B*). Coincubation with SB203580 or PD98059 abrogated stretch-induced TGF-β1 secretion (Fig. 5*A*). The results show that stretch-stimulated TGF-β1 secretion in UB cells was mediated by p38 and ERK.

Cyclic stretch induces apoptosis at 48 h via p38, ERK, and TGF-β in UB cells. Finally, we investigated whether cyclic stretch stimulates apoptosis in UB cells. At 24 h, percent apoptosis of stretched cells was not different from that of control cells (Fig. 6*A*). At 48 h, however, apoptosis was significantly increased by stretch (Fig. 6*B*). Stretch-induced apoptosis was abrogated by SB203580 or PD98059. Since TGF-β1 was increased by stretch, and TGF-β1 is a proapoptotic cytokine, the role of TGF-β1 in the stretch-induced apoptosis was examined using monoclonal anti-TGF-β-neutralizing antibody. As expected, anti-TGF-β antibody abrogated stretch-induced apoptosis in UB cells whereas nonspecific IgG had no effect. Under unstretched conditions, no difference in percent apoptosis was observed between control

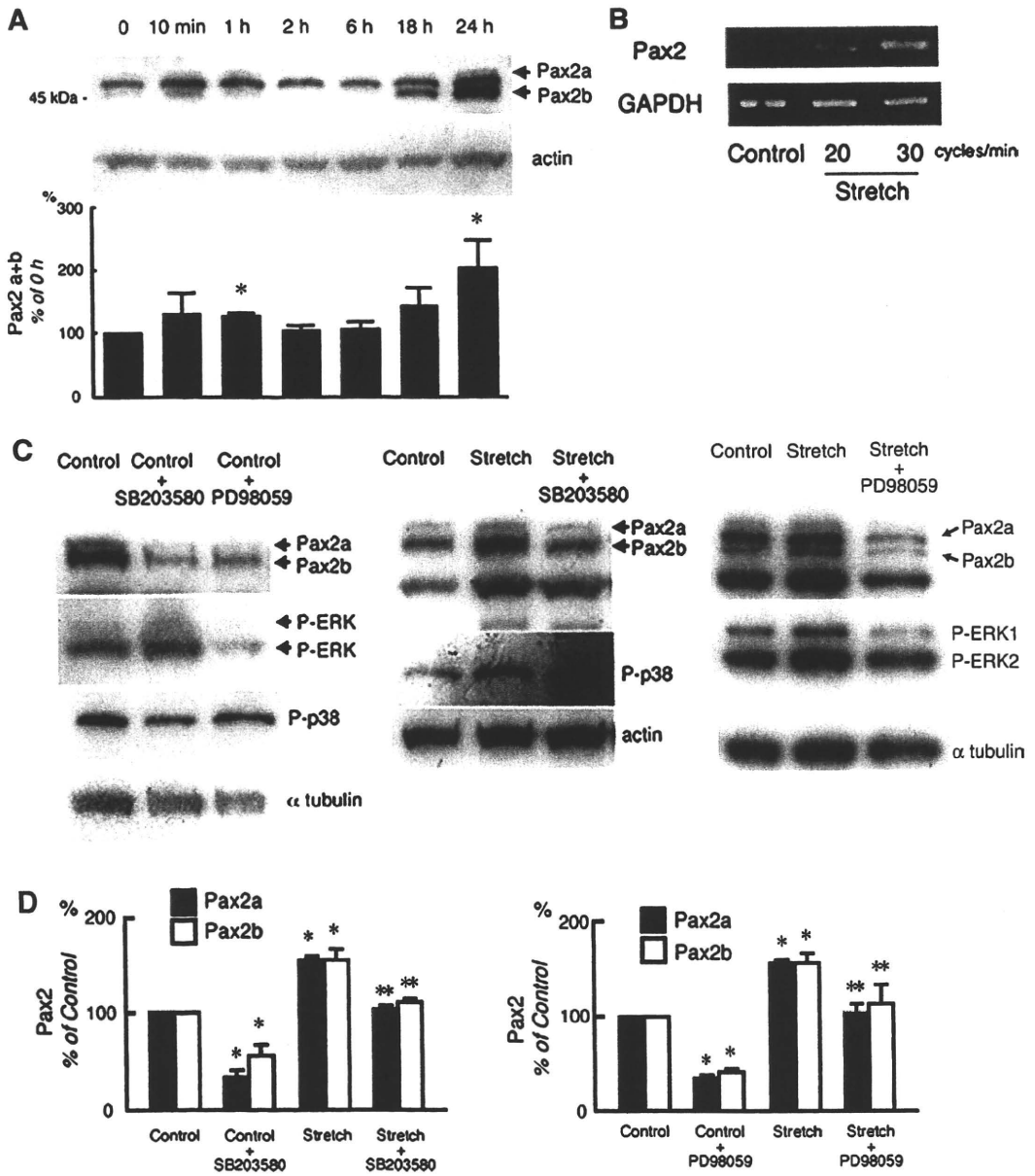

Fig. 3. Pax2 expression is increased by cyclic stretch via p38 and ERK in ureteric bud cells. *A*: ureteric bud cells were stretched 20 cycles/min for 0–24 h. Equal amounts of lysates (60 μg) were loaded and immunoblotted with anti-Pax2 antibody. Two isoforms of Pax2 were identified. *A*: representative immunoblot and quantitative analysis. *B*: Pax2 mRNA levels were detected by RT-PCR. *C*: cells were treated with a p38 inhibitor, SB203580, or a MEK inhibitor, PD98059, under unstretched conditions (*left*) or stretched for 24 h in the presence or absence of SB203580 (*middle*) or PD98059 (*right*). Representative immunoblots are shown. *D*: quantitative analyses. Values are means ± SE; $n = 3$. *$P < 0.05$ vs. control. **$P < 0.05$ vs. control+SB203580 or control+PD98059.

cells and cells treated with SB203580, PD98059, or anti-TGF-β antibody. While p38 and ERK mediate the stretch-induced TGF-β1 secretion, they may also serve as downstream signaling molecules of TGF-β1 in promoting apoptosis. To examine this possibility, the effect of exogenous TGF-β1 on UB cells was examined in the presence or absence of SB203580 or PD98059. TGF-β1 stimulated apoptosis of UB cells, which was completely inhibited by SB203580 or PD98059 (Fig. 7). These results demonstrate that p38 and ERK are both upstream and downstream signaling components of TGF-β1 in UB cells.

DISCUSSION

The present study demonstrates that cyclic stretching of UB cells, a mimic of fetal urinary tract obstruction, reproduces events seen in vivo. Thus p38 and ERK are activated by stretch and mediate Pax2 upregulation, cell proliferation, and secretion of TGF-β1, which subsequently induces apoptosis. p38 and ERK also serve as downstream molecules of TGF-β1 signaling (Fig. 8). The sequence of events is similar to that seen in in utero urinary tract obstruction. In our previous study in fetal lambs, cells positive for P-ERK, a proliferation marker Ki-67,

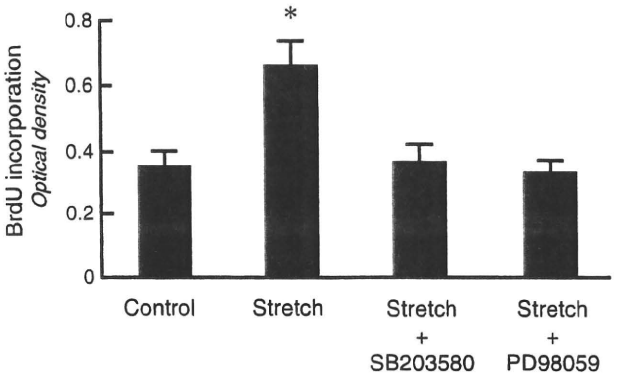

Fig. 4. p38 and ERK mediate cyclic stretch-induced 5-deoxyuridine (BrdU) incorporation. BrdU was added to the incubation media, and ureteric bud cells were stretched 20 cycles/min in the presence or absence of 5 μM SB203580 or 5 μM PD98059 for 24 h. BrdU incorporation was measured by a cell proliferation ELISA system. Values are means ± SE; $n = 7$. *$P < 0.05$ vs. control.

and TGF-β were observed in dilated tubules and cysts as early as 48 h after obstruction (23). Apoptosis in tubules and cysts, on the other hand, was detected 20 days after obstruction. This is in agreement with a previous study in adult rats, where cell proliferation preceded apoptosis after urinary tract obstruction (36). Proliferation was increased in tubules immediately after obstruction, whereas apoptosis was observed at *day 25*. The temporal relationship of these events has not been understood. The present study suggests that apoptosis is delayed because it

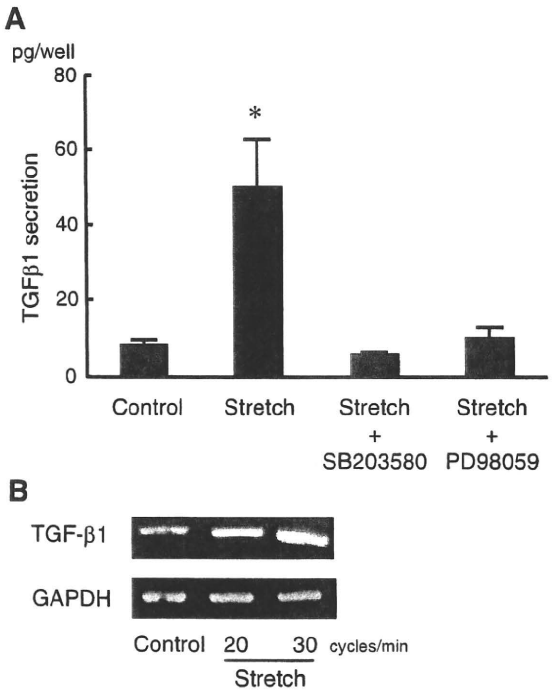

Fig. 5. p38 and ERK mediate cyclic stretch-induced transforming growth factor (TGF)-β1 secretion. *A*: ureteric bud cells were stretched 20 cycles/min in the presence or absence of 5 μM SB203580 or 5 μM PD98059 for 24 h. TGF-β1 in the medium was measured using ELISA kits. Values are means ± SE; $n = 3$. *$P < 0.05$ vs. control. *B*: TGF-β1 mRNA level was detected by RT-PCR.

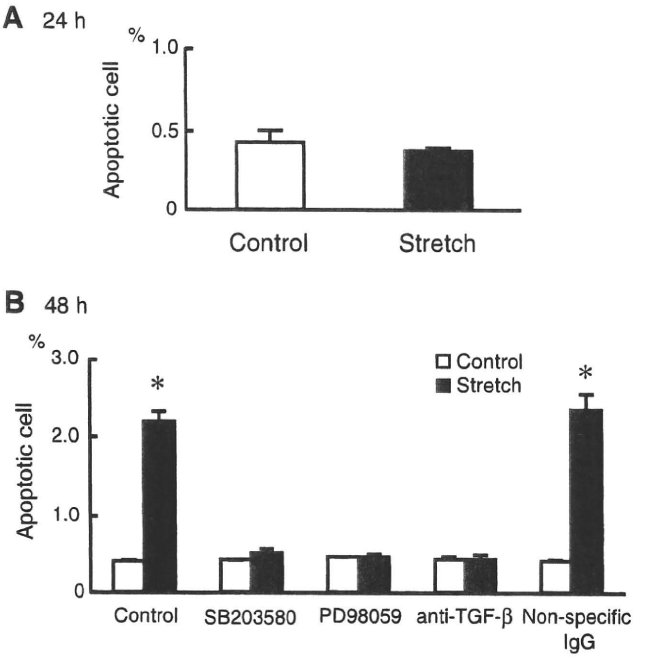

Fig. 6. Cyclic stretch increases apoptosis via p38 and ERK in ureteric bud cells. Ureteric bud cells were stretched 20 cycles/min for 24 (*A*) or 48 h (*B*). Apoptosis was determined by morphology using Hoechst 33258 staining. At 48 h, stretch increased apoptosis, which was inhibited by 5 μM SB203580, 5 μM PD98059, or 5 ng/ml anti-TGF-β1 antibody. Values are means ± SE; $n = 4$. *$P < 0.05$ vs. control.

is a secondary phenomenon induced by TGF-β1 secreted from tubules of the obstructed kidney.

In renal tubule cells, p38 and ERK have been shown to be activated by stretch in vitro or in vivo following obstruction (1, 16, 19, 33). In NRK-52E renal epithelial cells, p38 was activated by stretch and mediated apoptosis (19). The expression of p38 was increased in tubules of rat obstructed kidneys, and a p38 inhibitor ameliorated fibrosis (33). ERK, on the other hand, was activated by stretch via phospholipase A_2 in rabbit proximal tubule cells (1). In a rat unilateral ureteric obstruction model, the spatial pattern of ERK activation preceded that of BrdU incorporation, suggesting a role of ERK in cell prolifer-

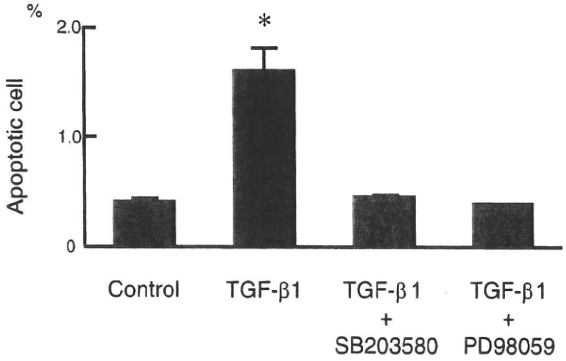

Fig. 7. TGF-β1 increases apoptosis via p38 and ERK in ureteric bud cells. Ureteric bud cells were incubated with 5 ng/ml TGF-β1 for 24 h in the presence or absence of 5 μM SB203580 or 5 μM PD98059. Apoptosis was determined by morphology using Hoechst 33258 staining. Values are means ± SE; $n = 4$. *$P < 0.05$ vs. control.

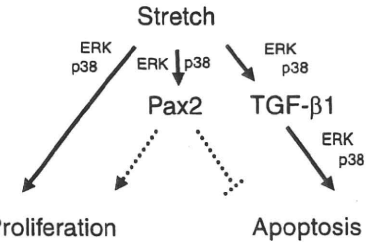

Fig. 8. The role of p38 and ERK in the stretch-induced proliferation and apoptosis of ureteric bud cells. Dashed lines are suggested from previous studies.

ation (16). We also showed that the temporospatial expression of P-ERK and that of p38, to a lesser extent, correlated with Ki-67 and TGF-β expression in an ovine model of fetal obstructive uropathy (23). These results suggest a role of ERK and p38 in cyst formation and fibrosis. The present study confirms that p38 and ERK mediate proliferation and TGF-β1 secretion induced by stretch. This is in contrast to the previous study by Stambe et al. (33) in adult rats, which showed that p38 blockade alleviated fibrosis without altering TGF-β1 expression. The discrepancy may be explained by differences in experimental design, degree of p38 inhibition, or tissue specificity.

TGF-β1 is a cytokine implicated in apoptosis, extracellular matrix deposition, and epithelial-mesenchymal transformation in various tissues. In NRK-52E renal epithelial cells, TGF-β1 was shown to be released by cell stretch and induce apoptosis (18). In the adult rat obstructed kidney, TGF-β was increased and administration of anti-TGF-β antibody diminished apoptosis and fibrosis (18). In a similar manner to adults, TGF-β1 may contribute to the pathogenesis of interstitial fibrosis, fibromuscular collar formation, and the maintenance of an undifferentiated state of cyst epithelium in obstructed fetal kidneys. Its protein and mRNA expression is upregulated in the epithelium of human renal dysplasia and an ovine model of fetal obstructive uropathy (23, 40). In a study by Yang et al. (40), TGF-β1 expression was correlated with that of α-smooth muscle actin (α-SMA), a marker of fibrosis, in tubules, cysts, and the interstitium in fetal urinary obstruction. They further demonstrated that TGF-β1 upregulated α-SMA in epithelial-like cells isolated from dysplastic kidneys (41). Also, the epithelial-mesenchymal transformation has been demonstrated in fetal urinary obstruction, which was associated with disruption of the epithelial basement membrane and migration of transitioning cells, resulting in the generation of peritubular collars of fibrous tissue (3). TGF-β1 has been demonstrated to induce epithelial mesenchymal transformation in collecting duct cells and Madin-Darby canine kidney (MDCK) cells (13, 30). These findings support the role of TGF-β1 in the pathogenesis of dysplasia.

p38 and ERK have been shown to mediate increases in TGF-β production by various stimuli in a number of cells. In mesangial cells, p38 mediated stretch-induced TGF-β1 production (9). In proximal tubule cells, both p38 and ERK mediated high glucose-stimulated TGF-β expression (8). The present study demonstrated that cyclic stretch stimulated TGF-β1 secretion via p38 and ERK in UB cells. p38 and ERK mediate proapoptotic and profibrotic effects of TGF-β1 as well. Thus we showed that p38 and ERK mediate the proapoptotic effect of TGF-β1. Stambe et al. (33) demonstrated that a p38 inhibitor reduced the expression of connective tissue growth factor, a downstream mediator of TGF-β1, in the obstructed adult kidney. TGF-β1 was shown to induce epithelial-mesenchymal transformation via p38 and ERK in NRK-52E cells and via ERK in MDCK cells (28, 30).

Pax2 is a transcription factor that plays an important role during kidney development. It is required for mesenchymal cell growth and prevention of apoptosis (6, 35). Pax2 knockout mice are characterized by hypoplasia and agenesis of the urogenital system (6). On the other hand, it is overexpressed in cyst epithelium of renal dysplasia, obstructed ovine fetal kidneys, and polycystic kidney disease (PKD), a condition characterized by the progressive expansion of multiple cysts which exhibit similar features to dysplasia i.e., increased proliferation and apoptosis (2, 23, 38, 39). Overexpression of Pax2 results in cystic diseases, whereas the reduction in Pax2 gene dosage decreased cyst formation in *cpk* mice, a murine model of rapid-onset PKD (5, 24). Pax2 is expressed in UBs and immature tubules during kidney development (23). In the adult kidney, its expression is confined to collecting ducts, a derivative of the UB, but becomes reexpressed in regenerating proximal tubules during experimental acute tubular necrosis (12). These findings suggest a role of Pax2 in cell proliferation. The expression and function of Pax2 are closely analogous to those of p38 and ERK. In cyst epithelium of fetal urinary tract obstruction, p38 and P-ERK are coexpressed with Pax2 (23). The inhibition of p38 and ERK disrupts normal kidney development in a similar matter to Pax2 deficiency. The present study demonstrates that the phosphorylation of p38 and ERK is correlated with Pax2 expression. Taken together, Pax2 expression in cyst epithelium of obstructed fetal kidneys is thought to be due to the activation of p38 and ERK.

While stretch-induced apoptosis has been shown, proliferation has not previously been demonstrated in vitro in renal epithelial cells. It is well known that stretch stimulates proliferation in cells of mesenchymal origin, including vascular smooth muscle cells, endothelial cells, myoblasts, and mesenchymal stem cells (10, 14, 32). In several of these cell types, stretch-induced proliferation is mediated by p38 or ERK (4, 14). The phenotypic characteristics of cells may affect the responses to stretch. It is possible that cells of mesenchymal origin or of immature fetal phenotype are more prone to proliferate in response to stretch. In this regard, it is of note that only fetal urinary tract obstruction at an early stage of development produces dysplastic kidneys (25). Obstruction at later stages results in hydronephrosis without abnormal parenchymal architecture. In obstructed adult kidneys, proliferation of tubule cells is seen only transiently at an early stage (36). In dysplastic kidneys, on the other hand, prominent proliferation persists beyond birth. Thus stretch-induced proliferation may be unique to UB cells or immature tubules and may be an important factor leading to dysplasia in in utero urinary obstruction. In support of this possibility, previous studies showed that proliferation is crucial for cyst development (15, 34).

We recently reported that the expression of MAPKs is also dysregulated in a murine model of PKD, DBA/2-*pcy/pcy* (*pcy*) mice (21). In renal cystic disease, fluid accumulation within cyst lumens might stretch cyst walls and activate p38 and ERK, which in turn stimulate cell proliferation. Administration of a

MEK inhibitor in *pcy* mice inhibited cyst formation and improved renal function, demonstrating the role of ERK in cyst formation in PKD. Similar therapeutic effects may be expected in fetal urinary tract obstruction and renal dysplasia. p38 blockade may also be beneficial in cystic diseases. While a previous study demonstrated the role of p38 in stretch-induced apoptosis and fibrosis in urinary obstruction, the present study suggests that p38 is also important in cell proliferation and probably for cyst formation (19). One has to keep in mind, however, that p38 or ERK inhibition disturbs normal nephrogenesis (11).

In conclusion, in vitro studies on cultured immature tubule cells in stretch devices have elucidated the mechanisms by which cells convert the mechanical stimulus into cellular responses. In utero urinary tract obstruction may modify the functions of renal tubule cells to activate p38 and ERK, which in turn stimulate proliferation and TGF-β1 secretion, leading to cyst formation and dysplastic changes. Elucidation of mechanisms leading to MAPK activation may allow development of novel therapeutic strategies for renal dysplasia without affecting normal kidney growth and differentiation.

ACKNOWLEDGMENTS

We thank Dr. J. Barasch for kindly providing the ureteric bud cells.

GRANTS

This study was supported by grants from the Ministry of Education, Science, and Culture, Japan (17591115, 18591225, 20591286) and the Pfizer Fund for Growth and Development Research. Portions of the results in this work were presented at Renal Week 2002, 2003, 2004 of the American Society of Nephrology, and published as an abstract in *J Am Soc Nephrol* 13: 104A, 2002; 14: 96A, 2003, and 15: 420A, 2004.

DISCLOSURES

No conflicts of interest, financial or otherwise, are declared by the authors.

REFERENCES

1. **Alexander LD, Alagarsamy S, Douglas JG.** Cyclic stretch-induced cPLA2 mediates ERK 1/2 signaling in rabbit proximal tubule cells. *Kidney Int* 65: 551–563, 2004.
2. **Attar R, Quinn F, Winyard PJ, Mouriquand PD, Foxall P, Hanson MA, Woolf AS.** Short-term urinary flow impairment deregulates PAX2 and PCNA expression and cell survival in fetal sheep kidneys. *Am J Pathol* 152: 1225–1235, 1998.
3. **Butt MJ, Tarantal AF, Jimenez DF, Matsell DG.** Collecting duct epithelial-mesenchymal transition in fetal urinary tract obstruction. *Kidney Int* 72: 936–944, 2007.
4. **Clause KC, Tinney JP, Liu LJ, Keller BB, Tobita K.** Engineered early embryonic cardiac tissue increases cardiomyocyte proliferation by cyclic mechanical stretch via p38-MAP kinase phosphorylation. *Tissue Eng Part A* 15: 1373–1380, 2009.
5. **Dressler GR, Wilkinson JE, Rothenpieler UW, Patterson LT, Williams-Simons L, Westphal H.** Deregulation of Pax-2 expression in transgenic mice generates severe kidney abnormalities. *Nature* 362: 65–67, 1993.
6. **Eccles MR.** The role of PAX2 in normal and abnormal development of the urinary tract. *Pediatr Nephrol* 12: 712–720, 1998.
7. **Edouga D, Hugueny B, Gasser B, Bussieres L, Laborde K.** Recovery after relief of fetal urinary obstruction: morphological, functional and molecular aspects. *Am J Physiol Renal Physiol* 281: F26–F37, 2001.
8. **Fujita H, Omori S, Ishikura K, Hida M, Awazu M.** ERK and p38 mediate high-glucose-induced hypertrophy and TGF-β expression in renal tubular cells. *Am J Physiol Renal Physiol* 286: F120–F126, 2004.
9. **Gruden G, Zonca S, Hayward A, Thomas S, Maestrini S, Gnudi L, Viberti GC.** Mechanical stretch-induced fibronectin and transforming growth factor- β1 production in human mesangial cells is p38 mitogen-activated protein kinase-dependent. *Diabetes* 49: 655–661, 2000.
10. **Haga JH, Li YS, Chien S.** Molecular basis of the effects of mechanical stretch on vascular smooth muscle cells. *J Biomech* 40: 947–960, 2007.
11. **Hida M, Omori S, Awazu M.** ERK and p38 MAP kinase are required for rat renal development. *Kidney Int* 61: 1252–1262, 2002.
12. **Imgrund M, Grone E, Grone HJ, Kretzler M, Holzman L, Schlondorff D, Rothenpieler UW.** Re-expression of the developmental gene Pax-2 during experimental acute tubular necrosis in mice. *Kidney Int* 56: 1423–1431, 1999.
13. **Ivanova L, Butt MJ, Matsell DG.** Mesenchymal transition in kidney collecting duct epithelial cells. *Am J Physiol Renal Physiol* 294: F1238–F1248, 2008.
14. **Kook SH, Lee HJ, Chung WT, Hwang IH, Lee SA, Kim BS, Lee JC.** Cyclic mechanical stretch stimulates the proliferation of C2C12 myoblasts and inhibits their differentiation via prolonged activation of p38 MAPK. *Mol Cells* 25: 479–486, 2008.
15. **Mangoo-Karim R, Uchic M, Lechene C, Grantham JJ.** Renal epithelial cyst formation and enlargement in vitro: dependence on cAMP. *Proc Natl Acad Sci USA* 86: 6007–6011, 1989.
16. **Masaki T, Foti R, Hill PA, Ikezumi Y, Atkins RC, Nikolic-Paterson DJ.** Activation of the ERK pathway precedes tubular proliferation in the obstructed rat kidney. *Kidney Int* 63: 1256–1264, 2003.
17. **Miyajima A, Chen J, Kirman I, Poppas DP, Darracott Vaughan EJ, Felsen D.** Interaction of nitric oxide and transforming growth factor-β1 induced by angiotensin II and mechanical stretch in rat renal tubular epithelial cells. *J Urol* 164: 1729–1734, 2000.
18. **Miyajima A, Chen J, Lawrence C, Ledbetter S, Soslow RA, Stern J, Jha S, Pigato J, Lemer ML, Poppas DP, Vaughan ED, Felsen D.** Antibody to transforming growth factor-β ameliorates tubular apoptosis in unilateral ureteral obstruction. *Kidney Int* 58: 2301–2313, 2000.
19. **Nguyen HT, Hsieh MH, Gaborro A, Tinloy B, Phillips C, Adam RM.** JNK/SAPK and p38 SAPK-2 mediate mechanical stretch-induced apoptosis via caspase-3 and -9 in NRK-52E renal epithelial cells. *Nephron Exp Nephrol* 102: e49–e61, 2006.
20. **Omori S, Fukuzawa R, Hida M, Awazu M.** Expression of mitogen-activated protein kinases in human renal dysplasia. *Kidney Int* 61: 899–906, 2002.
21. **Omori S, Hida M, Fujita H, Takahashi H, Tanimura S, Kohno M, Awazu M.** Extracellular signal-regulated kinase inhibition slows disease progression in mice with polycystic kidney disease. *J Am Soc Nephrol* 17: 1604–1614, 2006.
22. **Omori S, Hida M, Ishikura K, Kuramochi S, Awazu M.** Expression of mitogen-activated protein kinase family in rat renal development. *Kidney Int* 58: 27–37, 2000.
23. **Omori S, Kitagawa H, Koike J, Fujita H, Hida M, Pringle KC, Awazu M.** Activated extracellular signal-regulated kinase correlates with cyst formation and transforming growth factor-beta expression in fetal obstructive uropathy. *Kidney Int* 73: 1031–1037, 2008.
24. **Ostrom L, Tang MJ, Gruss P, Dressler GR.** Reduced Pax2 gene dosage increases apoptosis and slows the progression of renal cystic disease. *Dev Biol* 219: 250–258, 2000.
25. **Peters CA.** Obstruction of the fetal urinary tract. *J Am Soc Nephrol* 8: 653–663, 1997.
26. **Potter E.** *Normal and Abnormal Development of the Kidney.* Chicago, IL: Year Book, 1972.
27. **Quinlan MR, Docherty NG, Watson RW, Fitzpatrick JM.** Exploring mechanisms involved in renal tubular sensing of mechanical stretch following ureteric obstruction. *Am J Physiol Renal Physiol* 295: F1–F11, 2008.
28. **Rhyu DY, Yang Y, Ha H, Lee GT, Song JS, Uh ST, Lee HB.** Role of reactive oxygen species in TGF-β1-induced mitogen-activated protein kinase activation and epithelial-mesenchymal transition in renal tubular epithelial cells. *J Am Soc Nephrol* 16: 667–675, 2005.
29. **Richard MN, Deniset JF, Kneesh AL, Blackwood D, Pierce GN.** Mechanical stretching stimulates smooth muscle cell growth, nuclear protein import, and nuclear pore expression through mitogen-activated protein kinase activation. *J Biol Chem* 282: 23081–23088, 2007.
30. **Schramek H, Feifel E, Marschitz I, Golochtchapova N, Gstraunthaler G, Montesano R.** Loss of active MEK1-ERK1/2 restores epithelial phenotype and morphogenesis in transdifferentiated MDCK cells. *Am J Physiol Cell Physiol* 285: C652–C661, 2003.
31. **Shibata S, Shigeta M, Shu Y, Watanabe T, Nagata M.** Initial pathological events in renal dysplasia with urinary tract obstruction in utero. *Virchows Arch* 439: 560–570, 2001.

32. **Song G, Ju Y, Soyama H, Ohashi T, Sato M.** Regulation of cyclic longitudinal mechanical stretch on proliferation of human bone marrow mesenchymal stem cells. *Mol Cell Biomech* 4: 201–210, 2007.
33. **Stambe C, Atkins RC, Tesch GH, Masaki T, Schreiner GF, Nikolic-Paterson DJ.** The role of p38α mitogen-activated protein kinase activation in renal fibrosis. *J Am Soc Nephrol* 15: 370–379, 2004.
34. **Tanner GA, McQuillan PF, Maxwell MR, Keck JK, McAteer JA.** An in vitro test of the cell stretch-proliferation hypothesis of renal cyst enlargement. *J Am Soc Nephrol* 6: 1230–1241, 1995.
35. **Torban E, Eccles MR, Favor J, Goodyer PR.** PAX2 suppresses apoptosis in renal collecting duct cells. *Am J Pathol* 157: 833–842, 2000.
36. **Truong LD, Petrusevska G, Yang G, Gurpinar T, Shappell S, Lechago J, Rouse D, Suki WN.** Cell apoptosis and proliferation in experimental chronic obstructive uropathy. *Kidney Int* 50: 200–207, 1996.
37. **Warady BA, Hebert D, Sullivan EK, Alexander SR, Tejani A.** Renal transplantation, chronic dialysis, and chronic renal insufficiency in children and adolescents. The 1995 Annual Report of the North American Pediatric Renal Transplant Cooperative Study. *Pediatr Nephrol* 11: 49–64, 1997.
38. **Winyard PJ, Nauta J, Lirenman DS, Hardman P, Sams VR, Risdon RA, Woolf AS.** Deregulation of cell survival in cystic and dysplastic renal development. *Kidney Int* 49: 135–146, 1996.
39. **Winyard PJ, Risdon RA, Sams VR, Dressler GR, Woolf AS.** The PAX2 transcription factor is expressed in cystic and hyperproliferative dysplastic epithelia in human kidney malformations. *J Clin Invest* 98: 451–459, 1996.
40. **Yang SP, Woolf AS, Quinn F, Winyard PJ.** Deregulation of renal transforming growth factor-β1 after experimental short-term ureteric obstruction in fetal sheep. *Am J Pathol* 159: 109–117, 2001.
41. **Yang SP, Woolf AS, Yuan HT, Scott RJ, Risdon RA, O'Hare MJ, Winyard PJ.** Potential biological role of transforming growth factor-β1 in human congenital kidney malformations. *Am J Pathol* 157: 1633–1647, 2000.

The (Pro)renin Receptor/ATP6AP2 is Essential for Vacuolar H^+-ATPase Assembly in Murine Cardiomyocytes

Kenichiro Kinouchi, Atsuhiro Ichihara, Motoaki Sano, Ge-Hong Sun-Wada, Yoh Wada, Asako Kurauchi-Mito, Kanako Bokuda, Tatsuya Narita, Yoichi Oshima, Mariyo Sakoda, Yoshitaka Tamai, Hiromu Sato, Keiichi Fukuda, Hiroshi Itoh

Rationale: The (pro)renin receptor [(P)RR], encoded in *ATP6AP2*, plays a key role in the activation of local renin-angiotensin system (RAS). A truncated form of (P)RR, termed M8.9, was also found to be associated with the vacuolar H^+-ATPase (V-ATPase), implicating a non–RAS-related function of ATP6AP2.

Objective: We investigated the role of (P)RR/ATP6AP2 in murine cardiomyocytes.

Methods and Results: Cardiomyocyte-specific ablation of *Atp6ap2* resulted in lethal heart failure; the cardiomyocytes contained RAB7- and lysosomal-associated membrane protein 2 (LAMP2)-positive multivesicular vacuoles, especially in the perinuclear regions. The myofibrils and mitochondria remained at the cell periphery. Cardiomyocyte death was accompanied by numerous autophagic vacuoles that contained undigested cellular constituents, as a result of impaired autophagic degradation. Notably, ablation of *Atp6ap2* selectively suppressed expression of the V_O subunits of V-ATPase, resulting in deacidification of the intracellular vesicles. Furthermore, the inhibition of intracellular acidification by treatment with bafilomycin A1 or chloroquine reproduced the phenotype observed for the (P)RR/ATP6AP2-deficient cardiomyocytes.

Conclusions: Genetic ablation of *Atp6ap2* created a loss-of-function model for V-ATPase. The gene product of *ATP6AP2* is considered to act as in 2 ways: (1) as (P)RR, exerting a RAS-related function; and (2) as the V-ATPase-associated protein, exerting a non–RAS-related function that is essential for cell survival. (*Circ Res.* 2010;107:30-34.)

Key Words: V-ATPase ■ autophagy ■ heart failure ■ bafilomycin ■ renin-angiotensin system

Activation of the (pro)renin receptor [(P)RR], the gene product of ATP6AP2, plays a key role in the local renin-angiotensin system (RAS). We have shown that (P)RR activation is involved in the development of cardiac fibrosis and proteinuria in hypertension and diabetes. Interestingly, a truncated form of (P)RR, termed M8.9, was also found to be associated with the vacuolar H+-ATPase (V-ATPase), implicating a non–RAS-related function of the gene products of ATP6AP2.[1] In the present study, we show that gene products of ATP6AP2 are essential for cardiomyocyte survival via regulating V-ATPase function.

Methods

We generated conditional knockout (CKO) mice in which exon 2 of the *Atp6ap2* gene was flanked by loxP sites (Online Figure I). *Atp6ap2*-floxed mice were bred with mice that expressed the Cre recombinase under the control of the cardiomyocyte-specific α-myosin heavy chain (α-MHC) promoter (Online Figure II).[2,3] The resulting $Atp6ap2^{lox/Y}$, $\alpha MHC\text{-}Cre^{+/0}$ mice represent cardiac-specific *Atp6ap2* CKO mice. The control male mice were littermates that were heterozygous for α-MHC-Cre ($\alpha MHC\text{-}Cre^{+/0}$; $Atp6ap2^{+/Y}$), thereby excluding Cre-mediated toxicity as the basis for phenotypic disparity. An expanded Methods section is available in the Online Data Supplement at http://circres.ahajournals.org.

Results and Discussion

The CKO mice were born at the expected mendelian frequency, without any gross cardiac anomalies being noted in the newborn mice, although cardiomyocyte-specific ablation of *Atp6ap2* inevitably resulted in heart failure and the mice died within 3 weeks of birth (Figure 1a through 1c). Ventric-

Original received May 19, 2010; revision received June 1, 2010; accepted June 3, 2010. In May 2010, the average time from submission to first decision for all original research papers submitted to *Circulation Research* was 14.6 days.

From the Department of Endocrinology, Metabolism, and Nephrology (K.K., A.I., A.K.-M., K.B., T.N., M.S., H.I.), the Department of Endocrinology and Anti-Aging Medicine and Internal Medicine (A.I., Y.O.), and the Department of Cardiology (M.S., K.F.), Keio University School of Medicine, Tokyo, Japan; Precursory Research for Embryonic Science and Technology (PRESTO) (M.S.), Japan Science and Technology Agency, Saitama, Japan; the Department of Biochemistry (G.-H.S.-W.), Faculty of Pharmaceutical Sciences, Doshisha Women's College, Kyoto, Japan; the Division of Biological Sciences (Y.W.), Institute of Scientific and Industrial Research, Osaka University, Osaka, Japan; BANYU Tsukuba Research Institute (Y.T., H.S.), Ibaraki, Japan; and Charles River Laboratories JAPAN (Y.T.), Kanagawa, Japan.

Brief UltraRapid Communications are designed to be a format for manuscripts that are of outstanding interest to the readership, report definitive observations, but have a relatively narrow scope. Less comprehensive than Regular Articles but still scientifically rigorous, BURCs present seminal findings that have the potential to open up new avenues of research. A decision on BURCs is rendered within 7 days of submission.

Correspondence to Dr Atsuhiro Ichihara, Department of Endocrinology and Anti-Aging Medicine and Internal Medicine, Keio University School of Medicine, 35 Shinanomachi Shinjuku-ku, Tokyo, 160-8582, Japan. E-mail atzichi@sc.itc.keio.ac.jp

Circulation Research is available at http://circres.ahajournals.org DOI: 10.1161/CIRCRESAHA.110.224667

ular functions were severely impaired on postnatal day (PD)18 (fractional shortening, 12.87±4.73% versus 27.69±0.58% for CKO versus control; n=3; $P<0.05$) (Figure 1d, Online Video I). The CKO mice showed significantly increased ratios of heart weight—to–body weight beginning on PD14 (Figure 1e). The levels of cardiac stress markers, including atrial natriuretic peptide, brain natriuretic peptide, α-skeletal actin, connective tissue growth factor, and monocyte chemoattractant protein-1, were increased as early as PD10 (Figure 1f). Histological examination of the CKO mice on PD18 revealed that clusters of degenerating cardiomyocytes with extensive vacuolation, especially in the perinuclear region, were embedded in areas of replacement fibrosis (Figure 2a and 2b). Electron microscopic examination of the CKO cardiomyocytes revealed perinuclear accumulations of numerous multivesicular vacuoles (Figure 2c and 2d). The myofibrils and mitochondria were located exclusively at the cell periphery. In addition, we observed large, electron-dense autophagic vacuoles that contained partially digested or undigested cellular constituents, such as mitochondria and aberrant vacuoles, scattered in the field of cell debris around the perinuclear region (Online Figure III). The accumulation of microtubule-associated protein 1 light chain 3 (LC3)-II (a phosphatidylethanolamine conjugate) and p62/SQSTM1, as well as the induction of genes in response to amino acid starvation (eg, the genes for asparagine synthetase, activating transcription factor 4, and C/EBP homologous protein) reflected defective autophagic protein degradation in the CKO mice (Figure 2e and 2f).

To examine the underlying cellular mechanism responsible for cardiac death, we examined the role of the ATP6AP2 protein in the function of V-ATPase, which maintains a

Non-standard Abbreviations and Acronyms

α-MHC	α-myosin heavy chain
CKO	conditional knockout
LAMP2	lysosomal-associated membrane protein 2
LC3	microtubule-associated protein 1 light chain 3
MEFs	mouse embryonic fibroblasts
PD	postnatal day
(P)RR	(pro)renin receptor
RAS	renin-angiotensin system
V-ATPase	vacuolar H^+-ATPase

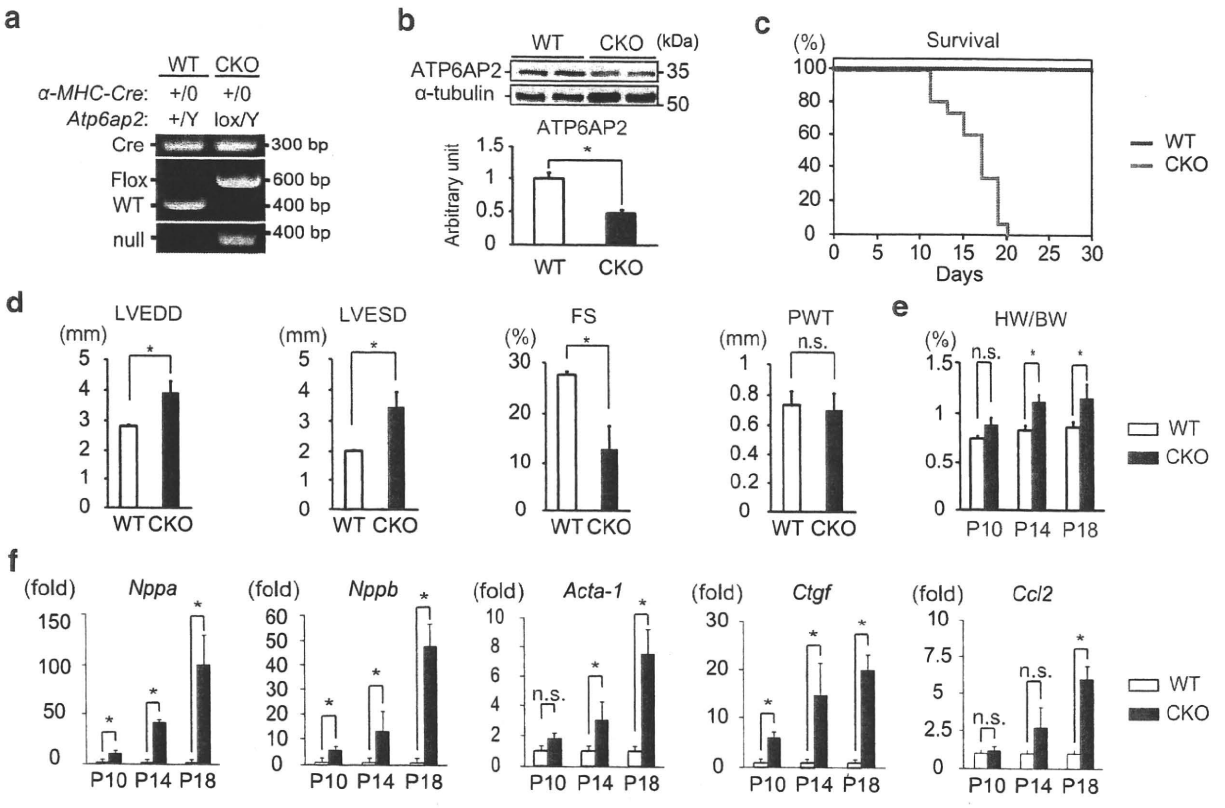

Figure 1. Cardiomyocyte-specific ablation of *Atp6ap2* inevitably caused heart failure. a, PCR genotyping of myocardial DNA, showing conditional deletion of floxed *Atp6ap2* contingent on coinheritance of *α-MHC-Cre*. **b**, ATP6AP2 protein was deleted from myocardium. *$P<0.05$ vs WT control. **c**, Kaplan-Meier survival curve showing lethality by 3 weeks of birth in the CKO mice. **d**, Echocardiographic data representing left ventricular dilation and compromised contraction in the CKO hearts on PD18. Values represent means±SEM. LVEDD indicates left ventricular end-diastolic diameter; LVESD, left ventricular end-systolic diameter; FS, fractional shortening; and PWT, posterior wall thickness. n=3, *$P<0.05$ vs WT control. **e**, HW/BW ratios of WT and CKO. n=4, *$P<0.05$ vs WT control. **f**, Expression of cardiac stress genes in the CKO mice. *Nppa* indicates atrial natriuretic peptide; *Nppb*, brain natriuretic peptide; *Acta-1*, α-skeletal actin; *Ctgf*, connective tissue growth factor; and *Ccl2*; monocyte chemotactic protein-1. n=4, *$P<0.05$ vs WT control.

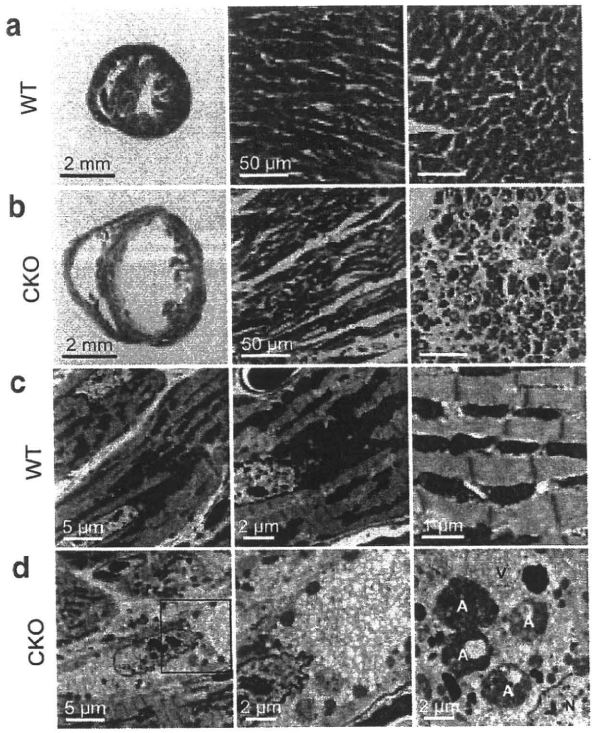

Figure 2. Extensive vacuolation of *Atp6ap2*-disrupted cardiomyocytes. a and b, Masson trichrome–stained, short-axis cross sections of the hearts of the CKO mice on PD18. **Scale bars:** 2 mm **(left panels)** and 50 μm **(center and right panels). c and d**, Ultrastructures of the vacuoles in the cardiomyocytes. **Scale bars:** 5 μm **(left panels),** 2 μm **(center panels);** 1 μm **(right upper panel),** and 2 μm **(right lower panel).** A indicates autophagic vacuole; and V, vesicular structure. **e**, Increased expression of LC3-II and p62 in ATP6AP2-depleted myocardium. *$P<0.05$ vs WT control. **f**, Expression of genes response to amino acid starvation in the CKO mice. *Asns* indicates asparagine synthetase; *Atf4*, activating transcription factor 4; and *Gadd153*, C/EBP homologous protein. n=4, *$P<0.05$ vs WT control.

luminal acidic environment in the intracellular vesicular compartments (Figure 3a).[4,5] Mouse embryonic fibroblasts (MEFs) were obtained from male mice that were hemizygous for the floxed *Atp6ap2* allele. The *Atp6ap2* gene was ablated by infecting the MEFs with the Cre adenovirus (Ad-Cre) (Online Figure IVa). Quantitative PCR and Western blot analyses showed that ≥90% of the ATP6AP2 protein was missing in the floxed MEFs after Ad-Cre treatment, as compared with the wild-type (WT) MEFs (Online Figure IVb and Figure 3b). V-ATPase is a large multisubunit complex that is organized into the V_1 and V_O sectors. In mammals, the V_1 sector is composed of 8 different subunits (A through H), whereas the V_O sector contains 6 different subunits (a, c, c″, d, e, and the accessory subunit Ac45[6]) (Figure 3a). Western blot and immunohistochemical analyses revealed that the levels of subunits a1, a2, a3, and c were significantly decreased in the floxed MEFs after Ad-Cre infection, as compared with the WT MEFs (Figure 3b and 3c). In contrast, the level of V_1 subunit E2 was unaffected. Consistent with these findings, LysoTracker staining revealed that the loss of ATP6AP2 was accompanied by impaired vesicular acidification (Figure 3c). Taken together, these findings suggest that genetic ablation of ATP6AP2 selectively affects the stability and assembly of the V_O subunits, thereby compromising vesicular acidification.

Consistent with the findings observed for cultured cells, ATP6AP2-depleted hearts revealed that the characteristic perinuclear vacuoles in the cardiomyocytes were positive for late endosomal/lysosomal markers RAB7 and/or LAMP2 (Figure 3d). The levels of the c-subunit of the V_O sector but not the E2 subunit of the V1 sector markedly reduced in the CKO cardiomyocytes.

To investigate whether disruption of intracellular acidification accounts for the phenotype of the ATP6AP2-deficient cardiomyocytes, we treated cultured cardiomyocytes with bafilomycin A1 or chloroquine. Sequential time-lapse microscopic analysis revealed that intracellular vacuoles accumulated over time (Figure 4; Online Video II). These vacuoles were positive for RAB7 (Figure 4). Interestingly, *Atp6ap2* mRNA expression in the cultured cardiomyocytes was strikingly upregulated after treatment with either bafilomycin A1 or chloroquine (Online Figure V).

The biogenesis of the multisubunit complex of V-ATPase requires the coordinated association of V_1 subunits, which are synthesized in the cytosol, with V_O subunits, which are targeted to the vacuolar membrane. Studies in yeast cells have shown that the loss of a V_1 subunit has little effect on the stability of the remaining V_1 subunit, whereas the loss of any single V_O subunit affects the stability and assembly of the remaining V_O subunits. In yeast, several additional genes (*Vma12p*, *Vma21p*, and *Vma22p*) that are required for V-ATPase assembly have been identified.[7] The V_O subunits were detected at greatly reduced levels in the mutant cells that lacked these assembly factors, an effect that is similar to that observed after the loss of a V_O subunit.[8] Interestingly, there is no known yeast homolog of the mammalian ATP6AP2. It is possible that ATP6AP2 is an assembly chaperone of V-ATPase, representing a function that is unique to mammals. An alternative scenario is that ATP6AP2 is a component of the V_O sector itself rather than an assembling factor. *Atp6ap2* mRNA expression was upregulated in cells that were treated with bafilomycin A1 or chloroquine, which suggests that ATP6AP2 senses the acidity levels of the intracellular compartments and accordingly regulates V-ATPase activity.

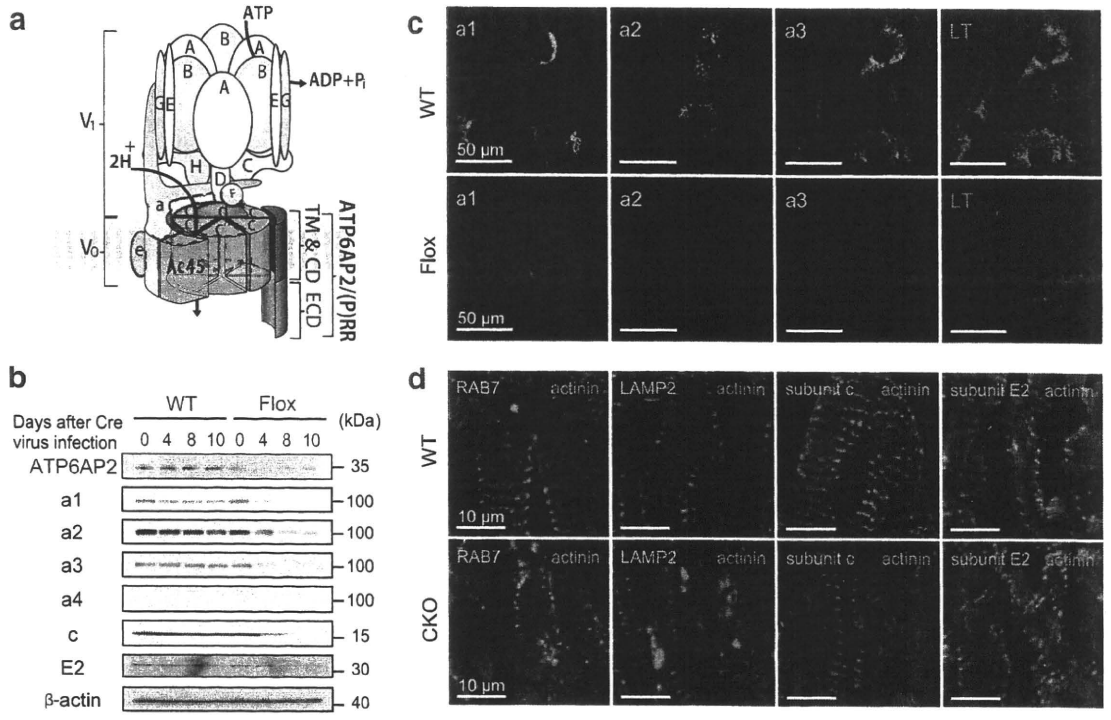

Figure 3. ATP6AP2 is indispensable for the assembly of V-ATPase. a, Structure of the V-ATPase and putative colocalization of ATP6AP2 and the V-ATPase. TM & CD indicates transmembrane and cytosolic domain; and ECD, extracellular domain. **b and c,** The levels of V_O subunits are decreased significantly in the floxed MEFs after deletion of the *Atp6ap2* gene. The V_1 subunit E2 appears to be unaffected. **c,** Defective acidification in the floxed MEFs after deletion of the *Atp6ap2* gene. **Scale bars:** 50 μm. **d,** Immunofluorescence staining of left ventricular tissues from WT and CKO mice on PD18. The vacuoles in the actinin-positive cardiomyocytes are RAB7-positive and LAMP2-positive. The levels of the c-subunit of the V_O sector of the V-ATPase are markedly reduced in the CKO cardiomyocytes, whereas the depletion of ATP6AP2 had no effect on the expression of the subunit E2 in cardiomyocytes. Nuclei were counterstained with DAPI **(blue). Scale bar:** 10 μm.

In conclusion, the gene product of *Atp6ap2* is considered to act in 2 ways: (1) as (P)RR, exerting an RAS-related function[9]; and (2) as the V-ATPase–associated protein, exerting a non–RAS-related function that is essential for cell survival.[10] The phenotypes observed after genetic ablation of *Atp6ap2* are ascribed to V-ATPase loss of function. Further characterizing the function of ATP6AP2 as an assembly chaperone of V-ATPase and the pathological function of

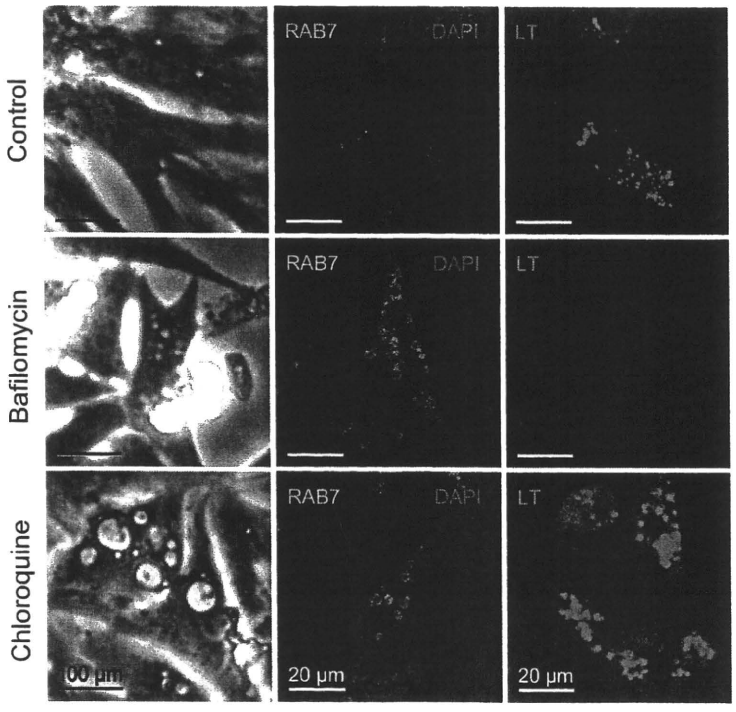

Figure 4. Inhibition of vesicular acidification by bafilomycin A1 or chloroquine mimics the in vivo cardiac phenotype that results from ablation of *Atp6ap2*. The rat cardiomyocytes were treated with bafilomycin A1 (100 nmol/L) or chloroquine (10 μmol/L) for 24 hours and then stained either with RAB7 plus DAPI or LysoTracker Red. Note that treatment with bafilomycin A1 or chloroquine reproduces the RAB7-positive intracellular vesicles by inhibiting vesicular acidification. **Scale bars:** 100 μm **(left panels)** and 20 μm **(center and right panels).**